

OPTIMAL CHEBYSHEV SMOOTHERS AND ONE-SIDED V-CYCLES*

MALACHI PHILLIPS[†] AND PAUL FISCHER^{†‡}

Abstract. The solution to the Poisson equation arising from the spectral element discretization of the incompressible Navier-Stokes equation requires robust preconditioning strategies. One such strategy is multigrid. To realize the potential of multigrid methods, effective smoothing strategies are needed. Chebyshev polynomial smoothing proves to be an effective smoother. However, there are several improvements to be made, especially at the cost of symmetry. For the same cost per iteration, a full V-cycle with k order Chebyshev polynomial smoothing may be substituted with a half V-cycle with order $2k$ Chebyshev polynomial smoothing, wherein the smoother is omitted on the up-leg of the V-cycle. The choice of omitting the post-smoother in favor of higher order Chebyshev pre-smoothing is shown to be advantageous in cases where the multigrid approximation property constant, C , is large. Results utilizing Lottes's fourth-kind Chebyshev polynomial smoother are shown. These methods demonstrate substantial improvement over the standard Chebyshev polynomial smoother. The authors demonstrate the effectiveness of this scheme in p -geometric multigrid, as well as a 2D model problem with finite differences.

Key words. multigrid, smoothers, parallel computing

MSC codes. 76D05, 65N55, 65F08

1. Introduction. Chebyshev smoothing was introduced in the context of parallel multigrid (MG) methods in [1], where it was established that Chebyshev smoothing was competitive with Gauss-Seidel smoothing even in serial computing applications. Here, we explore several variations on Chebyshev smoothing for the Poisson problem in general domains. Our primary aim is to develop fast highly-scalable solvers for the pressure sub-step in time advancement of the Navier-Stokes (NS) equations, particularly for discretizations based on the spectral element method (SEM). Many of the finding, however, would apply in more general settings.

Our target problem is to solve a sequence of Poisson problems,

$$(1.1) \quad -\nabla^2 \tilde{u} = \tilde{f} \text{ for } \tilde{u}, \tilde{f} \in \Omega \subset \mathbb{R}^d \mapsto \mathbb{R}.$$

The weak formulation is written as: *find* $u^m(\mathbf{x}) \in X_0^N \subset \mathcal{H}_0^1$ *such that*

$$(1.2) \quad \int_{\Omega} \nabla v \cdot \nabla u \, dV = \int_{\Omega} v f^m \, dV \quad \forall v \in X_0^N,$$

where $f^m(\mathbf{x})$ is the data and $u^m(\mathbf{x})$ is the corresponding solution field at some time instant t^m , $m = 1, 2, \dots$. Here, $\Omega \subset \mathbb{R}^d$ is the computational domain in d ($=1, 2$, or 3) space dimensions; $\mathcal{H}_0^1(\Omega)$ is the standard Sobolev space comprising functions that vanish on a subset of the boundary, $\partial\Omega_D \subset \partial\Omega$, are square-integrable on Ω , and whose gradient is also square-integrable; and $X_0^N = \text{span}\{\phi_j(\mathbf{x})\}$ is the finite-dimensional trial/test space associated with a Galerkin formulation of the Poisson problem. The discrete problem statement is expressed as $A\mathbf{u}^m = \mathbf{b}^m$, where \mathbf{u}^m is the vector of basis coefficients at t^m and A is the symmetric-positive definite (SPD) matrix with

$$(1.3) \quad a_{ij} = \int_{\Omega} \nabla \phi_i \cdot \nabla \phi_j \, dV.$$

*This work was funded by the Exascale Computing Project under contract no. 17-SC-20-SC

[†]Department of Computer Science, University of Illinois at Urbana-Champaign, Urbana IL 61801 (malachi2@illinois.edu).

[‡]Department of Mechanical Science and Engineering, University of Illinois at Urbana-Champaign, Urbana IL 61801 (fischerp@illinois.edu).

We point out that the need to solve a sequence of problems differs from solving a single problem in several significant ways. First, solver set-up costs are typically amortized over thousands of right-hand sides and are therefore largely irrelevant to our cost concerns. Second, the solution is typically devoid of significant low wave-number content because we solve only for a perturbed solution, $\delta \underline{u}^m := \underline{u}^m - \bar{\underline{u}}$, where $\bar{\underline{u}}$ is an initial guess. If we take $\bar{\underline{u}} = \underline{u}^{m-1}$ then the initial residual $r_0 = \underline{b} - A\underline{u}^{m-1} = O(\Delta t)$. This result is improved to $O(\Delta t^l)$ by projecting \underline{u}^m onto the space of prior solutions, $\{\underline{u}^{m-1} \dots \underline{u}^{m-l}\}$ [7, 16]. Finally, with an initially small residual, GMRES is likely to converge in just a few iterations, which obviates the need for restarts and mitigates the $O(k^2)$ complexity terms in a k -iteration GMRES solve. This latter observation puts less pressure on requiring a symmetric preconditioner since one can retain the full benefits of using Krylov subspace projection (KSP) without resorting to conjugate gradient iteration. With these circumstances in mind, we will drop the superscript m in the sequel.

We note that Chebyshev smoothers have gained a lot of attention recently. Kronbichler and co-workers [19, 11, 10] have employed Chebyshev smoothing for discontinuous Galerkin discretizations of the NS equations. Rudi and coworkers employ algebraic multigrid (AMG) with Chebyshev smoothing [32]. Similarly, Chebyshev smoothing is considered by Sundar and coworkers as a multigrid smoother for high-order continuous finite element discretizations [36].

A major difference here is that we consider Chebyshev in conjunction with additive Schwarz methods (ASM) [38, 12, 23, 30] and restrictive additive Schwarz (RAS) [5] in place of point-Jacobi smoothing. The principal idea is to use ASM or RAS to eliminate high wave number content. In the case of the spectral element method, local Schwarz solves can be effected at a cost that is comparable to forward operator evaluation through the use of fast diagonalization [24, 15, 23]. Another critical aspect of the current context is that many of our applications are targeting exascale platforms and beyond, where compute is performed on tens of thousands of GPUs for which the relative cost of global communication and hence, coarse-grid solves, is high [14]. In such cases, it often pays to have high-quality and broad bandwidth smoothing, such as provided by Chebyshev, in order to reduce the number of visits to the bottom of the V-cycle where the expensive coarse-grid solve is invoked.

Here, we explore a seemingly simple question: *Is it better to pre- and post-smooth k times each? Or to simply pre-smooth $2k$ times?* More specifically, in the Chebyshev context, the question is whether to use order k pre- and post-smoothing, or to only use order $2k$ presmoothing at the same cost per iteration. An additional and important point to this question is, *What kind of Chebyshev smoothing should be used?* One could use standard 1st-kind Chebyshev polynomials with tuned parameters. (Recall, we can afford significant tuning overhead.) Or, one could use standard or optimized 4th-kind Chebyshev polynomials that were proposed in recent work by Lottes. (See [22] and references therein.) We explore these questions under several different conditions: using finite differences and spectral elements discretizations and using Jacobi, ASM, or RAS as the basic smoother.

The structure of this paper is as follows. Section 2 outlines the multigrid V-cycle and Chebyshev smoothers. 2D finite difference Poisson results on varying aspect ratio grids, along with a comparison between theoretical and observed multigrid error contraction rates, are presented in section 3. Spectral element (SE)-based pressure Poisson preconditioning schemes implemented in the scalable open-source CFD code, nekRS [13], are presented in section 4. nekRS started as a fork of libParanumal [6] and uses highly optimized kernels based on the Open Concurrent Compute Abstrac-

tion (OCCA) [26]. Special focus is given to performance on large-scale GPU-based platforms such as OLCF's Summit. Cases for the stationary Poisson and pressure Poisson problem arising from the NS equations are shown in section 5. Results for the cases in section 5 are shown in section 6. Section 7 concludes the paper.

2. Multigrid and Chebyshev Smoothers. A denotes the SPD linear system to solve. Let P be the prolongation operator mapping degrees of freedom from the coarse grid to the fine grid. The Galerkin coarse grid operator is defined as $A_c := P^T A P$. The multigrid V-cycle is presented in Algorithm 2.1. How quickly does the V-cycle converge *as a solver*? Let us summarize the V-cycle theory by McCormick [25]. Multigrid seeks to decompose the solution space, \mathbb{R}^n , into the direct sum of the coarse grid space, which lies in the range of the prolongation operator, and the A -orthogonal complement of the coarse space,

$$\mathbb{R}^n = R(P) \oplus R(P)^{\perp_A}.$$

The pair of projectors for this decomposition are the coarse grid

$$\pi_c := P A_c^{-1} P^T A$$

and fine grid

$$\pi_f := I - \pi_c.$$

The two-level multigrid error propagator for the full V-cycle is

$$E_V = G'(I - P A_c^{-1} P^T A)G,$$

where G, G' are the iteration matrices for the pre- and post-smoother. For example, $G = (I - SA)^k$ for k steps of the iteration $\underline{x}_{k+1} = \underline{x}_k + S(\underline{b} - A\underline{x}_k)$. The error propagator for the full V-cycle can further be decomposed as the error propagator for the fine-to-coarse cycle

$$E = (I - P A_c^{-1} P^T A)G$$

and coarse-to-fine cycle

$$E' = G'(I - P A_c^{-1} P^T A).$$

Since $\pi_f := (I - P A_c^{-1} P^T A)$ is a projector with $\pi_f^2 = \pi_f$, $E_V = E'E$. For symmetric post-smoothing,

$$(2.1) \quad \|E_V\|_A = \|E\|_A^2$$

For the half V-cycle V' with no post-smoothing,

$$(2.2) \quad \|E_{V'}\|_A = \|E\|_A.$$

The multigrid approximation property constant is defined as

$$(2.3) \quad C := \|A^{-1} - P A_c^{-1} P^T\|_{A,S}^2 := \sup_{\|\underline{f}\|_S \leq 1} \|(A^{-1} - P A_c^{-1} P^T)\underline{f}\|_A^2.$$

where S denotes the smoother re-scaled such that $\rho(SA) = 1$. Following Lottes [22]:

$$(2.4) \quad C = \sup_{\underline{u} \in \mathbf{R}(\pi_f) \setminus 0} \frac{\|\underline{u}\|_{S^{-1}}^2}{\|\underline{u}\|_A^2} \geq 1.$$

The supremum in (2.4) over $\forall \underline{u} \neq 0$ is the reciprocal of the smallest eigenvalue of SA , which is $\kappa(SA)$, as $\rho(SA) = 1$. Therefore, $C \leq \kappa(SA)$. An imprecise interpretation of the multigrid approximation property constant, C , as described in (2.4), is the condition number of SA restricted to the A -orthogonal complement of the coarse grid space. By modifying Lanczos iteration on $(SA)^{-1}$ to project onto the A -orthogonal complement of the coarse grid space, the multigrid approximation property constant is estimated by the Ritz value from the iteration¹. Lottes derives upper bounds on the error contraction rate for multigrid *as a solver* with polynomial smoothers, Lemma 2.1 [22].

LEMMA 2.1. *Let the smoother iteration (on each level) be given by*

$$G = p_k(SA)$$

where S is SPD and scaled such that $\rho(SA) = 1$, and $p_k(x)$ is a k -order polynomial satisfying $p_k(0) = 1$ and $|p_k(x)| < 1$ for $0 < x \leq 1$, possibly different on each level. Then the V-cycle contraction factor

$$(2.5) \quad \|E\|_A(C, k)^2 \leq \max_{\text{levels}} \frac{C}{C + \gamma^{-1}}$$

$$(2.6) \quad := V(C, k),$$

where C is the approximation property constant, defined in (2.3), and

$$(2.7) \quad \gamma = \sup_{0 < \lambda \leq 1} \frac{\lambda p_k(\lambda)^2}{1 - p_k(\lambda)^2}.$$

Lottes notes that, for the simple damped smoother iteration $G = (I - \omega SA)^k$, $\gamma^{-1} \sim O(k)$. However, Chebyshev polynomials prove much more effective with $\gamma^{-1} \sim O(k^2)$.

Algorithm 2.1 Multigrid V-cycle

```

 $\underline{x} = \underline{x} + \text{presmooth}(A, \underline{x}_0, \underline{b})$ 
 $\underline{r} = \underline{b} - A\underline{x}, \underline{r}_C = P^T \underline{r}$ 
 $\underline{e}_C = A_C^{-1} \underline{r}_C$  // solve coarse system/re-apply multigrid
 $\underline{x} = \underline{x} + P \underline{e}$ 
 $\underline{x} = \underline{x} + \text{postsmooth}(A, \underline{x}, \underline{b})$ 

```

A notable improvement over the simple damped iteration is to use 1st-kind Chebyshev polynomials, as described in Algorithm 2.2 for a given smoother, S [1, 36]. While S is typically based on Jacobi smoothing (e.g., [19]), it is also possible to consider the use of ASM or RAS-based Chebyshev smoothing [30]. In order to apply the Chebyshev smoother, an eigenvalue estimate, $\tilde{\lambda}$, for $\lambda_{max}(SA)$ is needed. While λ_{max} is often chosen slightly larger than $\tilde{\lambda}$, such as $1.1\tilde{\lambda}$, multipliers for λ_{min} are more ad hoc. Previous works considered $(\lambda_{min}, \lambda_{max}) = (a\tilde{\lambda}, b\tilde{\lambda})$, with (a, b) constants as $(1/30, 1.1)$ [1], $(0.3, 1)$ [2], and $(0.25, 1)$ [36]. Two approaches utilizing the 1st-kind Chebyshev

¹See Algorithm 8.1 in the supplementary material for additional information.

smoother are considered in this study. The first uses $\lambda_{min} = 0.1\tilde{\lambda}$ and is denoted as 1st-Cheb. The second optimizes the multiplier value $\lambda_{min} = c\tilde{\lambda}$ and is denoted as 1st-Cheb, λ_{min}^{opt} .

To avoid the use of the ad hoc parameter λ_{min} , Lottes developed Chebyshev smoothers based on the 4th-kind Chebyshev polynomials, shown in Algorithm 2.3. In the 4th-kind Chebyshev smoother, denoted as 4th-Cheb, $\beta_i := 1$. In the optimized 4th-kind Chebyshev smoother, 4th_{opt}-Cheb, the β_i coefficients are chosen to minimize the error bound presented later in Lemma 2.1. Tabulated values for β_i are shown in the supplementary materials, Table 5. In the optimal 4th-kind Chebyshev smoother, denoted as 4th_{opt}-Cheb, the β_i parameters are chosen to minimize the error bound in Lemma 2.1. Lottes reports for the 4th-kind Chebyshev smoother

$$(2.8) \quad \gamma^{-1} = \frac{4}{3}k(k+1)$$

and optimized 4th-kind Chebyshev smoother

$$(2.9) \quad \gamma^{-1} \sim \frac{4}{\pi^2}(2k+1)^2 - \frac{2}{3}.$$

For the 1st-kind Chebyshev smoother, γ^{-1} is computed numerically. In addition, the 1st-kind Chebyshev smoother with λ_{min} chosen to minimize the error bound presented in Lemma 2.1 is also considered. All the Chebyshev schemes considered exhibit $\gamma^{-1} \sim O(k^2)$ scaling as $k \rightarrow \infty$.

Careful analysis of Algorithms 2.1 to 2.3, with $\underline{x}_0 = \underline{0}$ in Algorithm 2.1, show that k -order symmetric Chebyshev smoothing has the same cost as one-sided $2k$ -order Chebyshev smoothing. What effect does the one-sided approach have on the multigrid error contraction rate? To determine whether one-sided V-cycle with order $2k$ Chebyshev smoothing outperforms the symmetric V-cycle with order k Chebyshev smoothing, one must compare $\|E\|_A^2(C, k)$ to $\|E\|_A(C, 2k)$. Directly equating the bounds from Lemma 2.1 as an *approximation* for the multigrid error contraction factor, the (C, k) values at which $V(C, k) = \sqrt{V(C, 2k)}$ may be tabulated. These results, however, are deferred until section 3, to enable comparison against a numerical example.

A natural next question is on the expected improvement using the one-sided V-cycle provides. Using the bounds provided by Lemma 2.1 as a surrogate for the multigrid error contraction factor, the quantity $V(C, k)/\sqrt{V(C, 2k)}$ provides the expected performance gain using the one-sided V-cycle. For fixed k

$$\lim_{C \rightarrow \infty} \frac{V(C, k)}{\sqrt{V(C, 2k)}} = \frac{C}{C + \gamma^{-1}(k)} \cdot \frac{\sqrt{C + \gamma^{-1}(2k)}}{\sqrt{C}} = 1$$

With $C = 1$,

$$\lim_{k \rightarrow \infty} \frac{V(1, k)}{\sqrt{V(1, 2k)}} = \frac{\sqrt{1 + \gamma^{-1}(2k)}}{1 + \gamma^{-1}(k)} = 0$$

since γ^{-1} scales as $O(k^2)$ in the limit as $k \rightarrow \infty$. Between these two extremes, however, there is a potential benefit in using the one-sided V-cycle approach for moderate C . These results are deferred to section 3.

Algorithm 2.2 Chebyshev smoother, 1st-kind

$$\theta = \frac{1}{2}(\lambda_{max} + \lambda_{min}), \delta = \frac{1}{2}(\lambda_{max} - \lambda_{min}), \sigma = \frac{\theta}{\delta}, \rho_0 = \frac{1}{\sigma}$$

$$\underline{x}_0 = \underline{x}, r_0 = S(\underline{b} - A\underline{x}_0), \underline{d}_0 = \frac{1}{\theta}r_0$$
for $i = 1, \dots, k-1$ **do**

$$\underline{x}_i = \underline{x}_{i-1} + \underline{d}_{i-1}$$

$$r_i = r_{i-1} - S A \underline{d}_{i-1}, \rho_i = \frac{1}{2\sigma - \rho_{i-1}}$$

$$\underline{d}_i = \rho_i \rho_{i-1} \underline{d}_{i-1} + \frac{2\rho_i}{\delta} r_i$$
end for

$$\underline{x}_k = \underline{x}_{k-1} + \underline{d}_{k-1}$$
return \underline{x}_k

Algorithm 2.3 Chebyshev smoother, (Opt.) 4th-kind

$$\underline{x}_0 = \underline{x}, r_0 = \underline{b} - A\underline{x}_0$$

$$\underline{d}_0 = \frac{4}{3} \frac{1}{\lambda_{max}} r_0$$
for $i = 1, \dots, k-1$ **do**

$$\underline{x}_i = \underline{x}_{i-1} + \beta_i \underline{d}_{i-1}, r_i = r_{i-1} - A \underline{d}_{i-1}$$

$$\underline{d}_i = \frac{2i-1}{2i+3} \underline{d}_{i-1} + \frac{8i+4}{2i+3} \frac{1}{\lambda_{max}} S r_i$$
end for

$$\underline{x}_k = \underline{x}_{k-1} + \beta_k \underline{d}_{k-1}$$
return \underline{x}_k

3. Finite Differences with Geometric Multigrid Poisson. The Poisson equation (1.1) is considered with $d = 2$. Let $\Omega := [0, L_x] \times [0, L_y]$ be the domain of interest, with the boundary condition $u|_{\partial\Omega} = 0$. A finite difference grid of $(n+1) \times (n+1)$ points is considered, $n = 128$. For the purposes of this study, $u(x, y) = \sin(3\pi x/L_x) \sin(4\pi y/L_y) + g$, where g is the same random vector with $g|_{\partial\Omega} = 0$. $L_x \geq 1$ is varied, while L_y is fixed at unity. It follows that the aspect ratio of the grid is L_x . A two-level multigrid scheme with Chebyshev-accelerated Jacobi smoothing is employed as a preconditioner for a KSP. For the comparison with the bounds presented in Lemma 2.1, multigrid is also considered as a solver. The coarse level is discretized as $(n_c+1) \times (n_c+1)$, with $n_c = n/2$, as well as aggressive coarsening with $n_c = n/16$. As this case is meant to represent our target problem for *unstructured* multigrid, semi-coarsening is not employed. The coarse grid problem, $(PAP^T)^{-1}r_c$, is solved exactly. We choose a relative residual reduction of 10^{-6} as the stopping criterion. For the 1st-Cheb, λ_{min}^{opt} , a random right-hand side is used to tune λ_{min} . The multigrid approximation property constant is estimated using 20 Lanczos iterations, Algorithm 8.1.

Convergence results are based on the observed average solver convergence rate

$$(3.1) \quad \rho = \exp \left(\frac{1}{N} \log \frac{\|\underline{r}_N\|}{\|\underline{r}_0\|} \right),$$

where N is the number of iterations. The convergence rate for the full V-cycle is denoted $\rho_V(C, k)$, while the one-sided V-cycle is $\rho_{\searrow}(C, 2k)$. Values of (C, k) at which $\rho_V(C, k) \geq \rho_{\searrow}(C, 2k)$ are shown in Figure 1. Predicted results are from computing the smallest value C^* such that $V(C^*, k) \geq \sqrt{V(C^*, 2k)}$, Lemma 2.1, which is only applicable to multigrid as a *solver*, not *preconditioner*. Observed results are from 2D finite difference example. At a given k , $C > C^*$ indicates that the half V-cycle yields

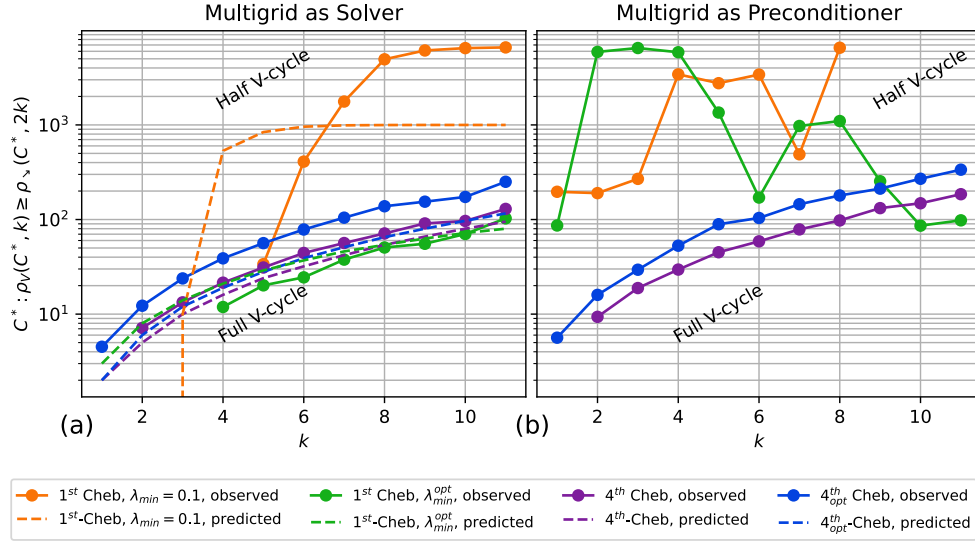


Fig. 1: Critical C^* at which the $2k$ -order one-sided Chebyshev converges faster for $C > C^*$.

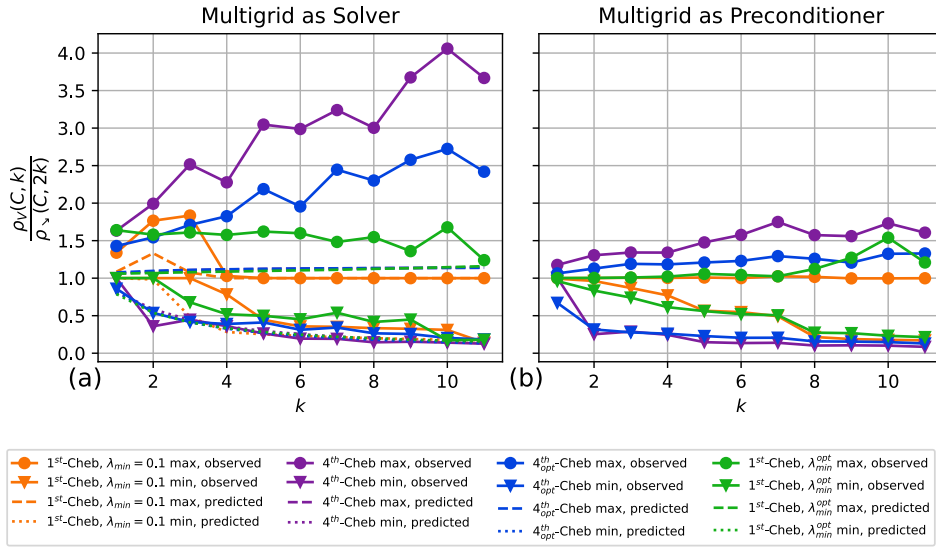


Fig. 2: Max (min) error contraction rate ratios for the full V-cycle and the one-sided V-cycle.

a lower error bound than the full V-cycle. Conversely, $C < C^*$, indicates that the full V-cycle yields better convergence. For the 1st-kind with optimized λ_{min} coefficient, 4th-kind, and optimized 4th-kind Chebyshev smoothers, the predicted domain in which to apply the one-sided V-cycle shows agreement with the results obtained by experiment using multigrid as a solver (Figure 1a). Remarkably, this analysis remains consistent for the 4th and optimized 4th-kind Chebyshev smoothers when considering the use of multigrid as a preconditioner (Figure 1b).

The maximum and minimum ratio of the error contraction rates, along with the predicted performance, are shown in Figure 2. While the predicted performance benefit of applying the one-sided V-cycle approach is limited, nevertheless, Figure 2a and Figure 2b demonstrate that the one-sided V-cycle offers an improvement compared

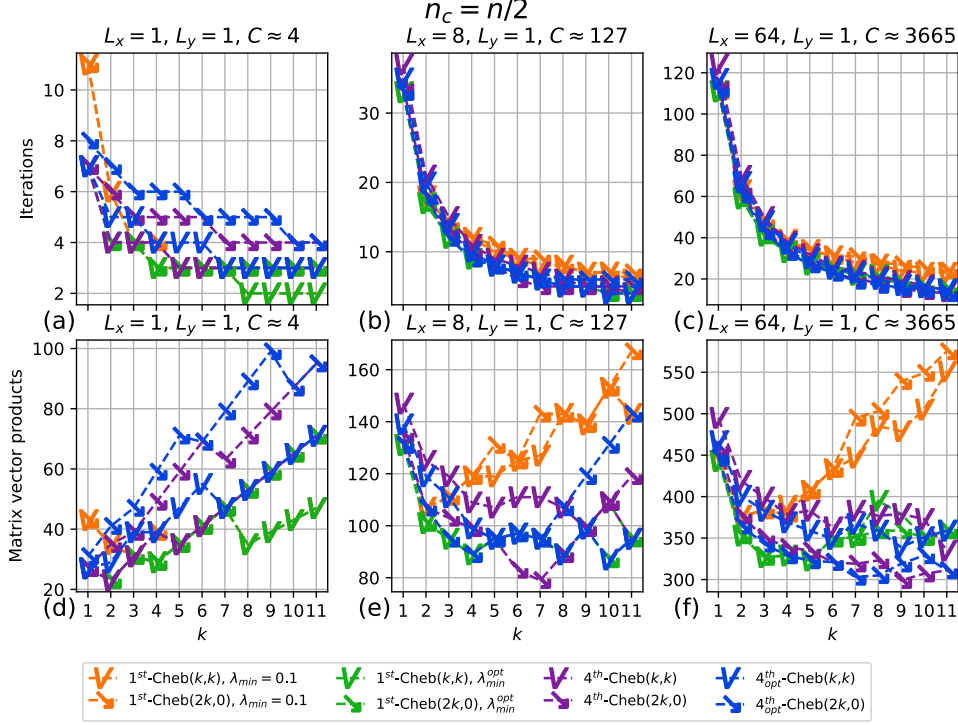


Fig. 3: FD, $n_c = n/2$. Multigrid as preconditioner for KSP.

to the full V-cycle for problems with moderate values of C . However, when applied to relatively easy problems ($C \approx 1$), the one-sided V-cycle is a poor choice.²

Results for $n_c = n/2$ are shown in Figure 3, $n_c = n/16$ in Figure 4. In both, multigrid is used to precondition the KSP solver³. In the case $n_c = n/2$ and $L_x = 1$ ($C \approx 4$), shown in Figure 3a,d, the work required, as measured by fine-grid matrix vector products, is minimized for relatively low orders. Further, applying the theoretical bounds shown in Figure 1a, this is the scenario in which the one-sided V-cycle approach *should not* be utilized. However, even at moderate grid aspect ratios, such as $L_x = 8$, $C \approx 127$ becomes large enough to justify the usage of the one-sided V-cycle approach, especially for the 4th-kind Chebyshev smoothers (Figure 3b,e) at moderate orders $k = 6, k = 12$. This effect becomes even more apparent when $L_x = 64$ ($C \approx 3665$), shown in Figure 3c,f. In the results for $n_c = n/2$, the 1st-kind with optimized λ_{min} , 4th-kind, and optimized 4th-kind Chebyshev smoothers greatly outperform the 1st-kind Chebyshev smoother, *especially* at high orders. Further, it is observed that both the iteration count and *total work* in matrix-vector products is minimized at high orders for the 1st-kind with optimized λ_{min} , 4th-kind, and optimized 4th-kind Chebyshev smoothers. This is not the case for the 1st-kind Chebyshev smoother. This effect of lowering both the iteration count and work has the additional benefit of reducing the number of coarse grid solves required for each iteration, whose cost is not factored in this analysis.

²Figure 15 shows the predicted and observed maximizer (minimizer) C where ratio between the one-sided and full V-cycle approaches is maximized (minimized).

³The same results, with multigrid as a solver, are shown in the supplementary materials, Figure 16, Figure 17.

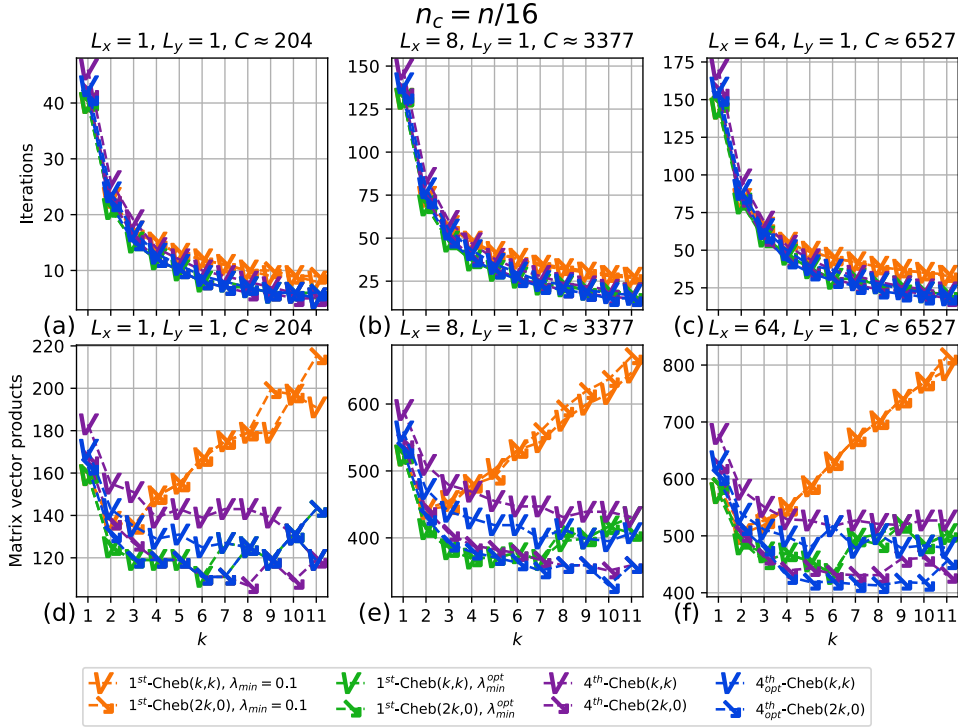


Fig. 4: FD, $n_c = n/16$. Multigrid as preconditioner for KSP.

In the aggressive coarsening case ($n_c = n/16$), both the number of matrix-vector products and iterations are reduced through using higher-order Chebyshev smoothing irrespective of the grid aspect ratio for all but the standard 1st-kind Chebyshev smoothers. Secondly, the one-sided V-cycle approach generally outperforms the full V-cycle approach, even for the unity grid aspect ratio case! There are two important implications from this result: first, there exists considerable benefit in transitioning a multigrid solver to either construct high-quality estimates for $\lambda_{\min}^{\text{opt}}$ for the 1st-kind Chebyshev smoother⁴ or utilize one of the 4th-kind Chebyshev smoothers; and second, additional performance can be achieved by using the one-sided V-cycle approach at the expense of symmetry, the implication of which is further discussed in subsection 6.1. Lastly, let us consider the trade-offs associated with using $n_c = n/2$ and $n_c = n/16$. Despite improvements in the convergence rate from using a different V-cycle approach or Chebyshev smoother, the number of matrix-vector products required by the solve is greater for the aggressive coarsening case. However, the relative cost per each coarse grid solve for $n_c = n/2$ compared to $n_c = n/16$ may be sufficient to justify the aggressive coarsening strategy, especially in a parallel computing context where each additional multigrid level requires additional communication cost. Significant effort has been spent on improving the parallel scalability of multigrid methods, especially in the AMG context, see [35, 9, 4]. One strategy to achieve better scalability is to rely on aggressive coarsening strategies, which require more robust smoothers, such as the Chebyshev smoothers discussed here.

⁴A record of the optimal $\lambda_{\min}^{\text{opt}}$ values for the 1st-kind Chebyshev smoother for finite differences are reported in the supplementary material, Figure 18.

L_x	Factor	Solver	Mat-Vec	Iterations
1	2	1 st -Cheb, λ_{min}^{opt} , Jacobi(2,2)	23	4
8	2	4 th -Cheb, Jacobi(14,0)	79	5
64	2	4 th -Cheb, Jacobi(18,0)	299	15
128	2	4 th _{opt} -Cheb, Jacobi(18,0)	319	16
1	16	4 th -Cheb, Jacobi(16, 0)	107	6
8	16	4 th _{opt} -Cheb, Jacobi(20, 0)	329	15
64	16	4 th _{opt} -Cheb, Jacobi(16, 0)	413	23
128	16	4 th _{opt} -Cheb, Jacobi(18, 0)	359	18

Table 1: Solver configuration with lowest number of matrix-vector products for finite difference geometric multigrid.

The results shown in Figure 3 and Figure 4 are summarized in Table 1. The solver configuration yielding the lowest number of matrix-vector products is listed for each case. 4th_{opt}-Cheb, Jacobi(18,0), for example, denotes a 18th order Chebyshev smoother of the optimized 4th-kind, using one-sided smoothing (thereby, having the same cost per iteration as order 9 with the full V-cycle). This solver configuration yields the lowest number of matrix-vector products for $L_x = 128$ with aggressive coarsening. We see that, for high aspect ratio grids and aggressive coarsening, the half V-cycle offers superior performance.

4. High Order Preconditioners. Let us now consider preconditioners for the Poisson equation (1.1) for $d = 3$ arising from the spectral element method (SEM) discretization of the incompressible NS equation, which typically encompasses the majority of the solution time in nekRS [13]. Two classes of preconditioners prove most effective: p -geometric multigrid (pMG) and low-order discretizations.

4.1. p -Geometric Multigrid. p -geometric multigrid (pMG) is used as a preconditioner for the Pressure poisson equation discretized using the spectral element method. Since the multigrid hierarchy is constructed by varying the polynomial order, p , of each level, geometric coarsening can be robustly applied up to $p = 1$, even in the *unstructured* case. Typical multigrid schedules for $p = 7$, for example, are V-cycles with orders (7, 5, 3, 1) or (7, 3, 1). In addition to the Chebyshev-accelerated Jacobi smoother, Chebyshev-accelerated Schwarz smoothers are also considered, as discussed in [30]. The Schwarz smoothers are outlined below.

The SE-based additive Schwarz method (ASM) presented in [23, 21] solves local Poisson problems on subdomains that are extensions of the spectral elements. The formal definition of the ASM preconditioner (or, in this case, pMG smoother) is

$$(4.1) \quad S_{ASM} \underline{r} = \sum_{e=1}^E W_e R_e^T \bar{A}_e^{-1} R_e \underline{r},$$

where R_e is the restriction matrix that extracts nodal values of the residual vector that correspond to each overlapping domain. To improve the smoothing properties of the ASM, we introduce the diagonal weight matrix, W_e , which scales each nodal value by the inverse of the number of subdomains that share that node. Although it compromises symmetry, post-multiplication by W_e was found to yield superior results to pre- and post-multiplication by $W_e^{\frac{1}{2}}$ [34, 23].

In a standard Galerkin ASM formulation, one would use $\bar{A}_e = R_e A R_e^T$, but such an approach would compromise the $O(p^3)$ storage complexity of the SE method. To

construct fast inverses for \bar{A}_e , we approximate each deformed element as a simple box-like geometry. These boxes are then extended by a single degree-of-freedom in each spatial dimension to form overlapping subdomains with $\bar{p}^3 = (p+3)^3$ interior degrees-of-freedom in each domain. The approximate box domain enables the use of the fast diagonalization method (FDM) to solve for each of the overlapping subdomains, which can be applied in $O(Ep^4)$ time in \mathbb{R}^3 . The extended-box Poisson operator is

$$\bar{A} = B_z \otimes B_y \otimes A_x + B_z \otimes A_y \otimes B_x + A_z \otimes B_y \otimes B_x,$$

where each B_*, A_* represents the extended 1D mass-stiffness matrix pairs along the given dimension [8]. The FDM begins with a preprocessing step of solving a series of small, $\bar{p} \times \bar{p}$, generalized eigenvalue problems,

$$A_* \underline{s}_i = \lambda_i B_* \underline{s}_i$$

and defining $S_* = (\underline{s}_1 \dots \underline{s}_{\bar{p}})$ and $\Lambda_* = \text{diag}(\lambda_i)$, to yield the similarity transforms

$$S_*^T A_* S_* = \Lambda_*, \quad S_*^T B_* S_* = I.$$

From these, the inverse of the local Schwarz operator is

$$\bar{A}^{-1} = (S_z \otimes S_y \otimes S_x) D^{-1} (S_z^T \otimes S_y^T \otimes S_x^T),$$

where D is a diagonal matrix defined as

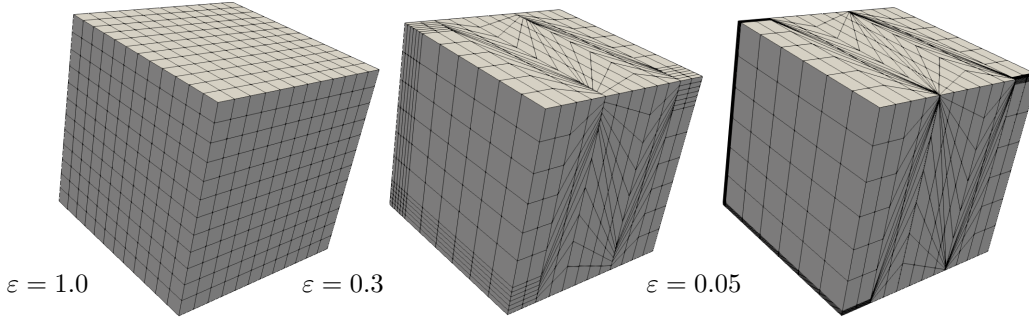
$$D := I \otimes I \otimes \Lambda_x + I \otimes \Lambda_y \otimes I + \Lambda_z \otimes I \otimes I.$$

This process is repeated for each element, at each multigrid level save for the coarsest one. Note that the per-element storage is only $3\bar{p}^2$ for the S_* matrices and \bar{p}^3 for D . At each multigrid level, the local subdomain solves are used as a smoother. On the coarsest level ($p = 1$), however, BoomerAMG [39] is used to solve the system on the CPU with the same parameters described in subsection 4.2, except using Chebyshev smoothing. A single BoomerAMG V-cycle iteration is used in the coarse-grid solve.

Presently, we also consider a restrictive additive Schwarz (RAS) version of (4.1), wherein overlapping values are not added after the action of the local FDM solve, following [5]. RAS has the added benefit of reducing the amount of communication required in the smoother. Similar to ASM, RAS is *non-symmetric*. Attempts to symmetrize the operator tend to have a negative impact on the convergence rate [5]. The smoother S_{ASM} or S_{RAS} described here is then used as the smoother considered in Chebyshev-acceleration, as shown in Algorithm 2.3 and Algorithm 2.2. The multigrid schedule for the cases in section 5 are $(7, 5, 3, 1)$ and $(7, 3, 1)$ for Chebyshev-Jacobi and Chebyshev-Schwarz respectively.

4.2. Preconditioning with Low Order Operators. In [28], Orszag suggested that constructing a sparse preconditioner based on the low-order discretizations with nodes coinciding with those of the high-order discretization would yield bounded condition numbers and, under certain constraints, can yield $\kappa(M^{-1}A) \sim \pi^2/4$ for second-order Dirichlet problems. This observation has led to the development of preconditioning techniques based on solving the resulting low-order system [29, 27, 3].

In the current work, we employ the same low-order discretization considered in [3]. Each of the vertices of the hexahedral element is used to form one low-order,

Fig. 5: Kershaw, $E = 12^3$, $p = 1$.

tetrahedral element, resulting in a total of eight low-order elements for each GLL sub-volume in each of the high-order hexahedral elements. This low-order discretization is then used to form the sparse operator, A_F . The so-called weak preconditioner, A_F^{-1} , is used to precondition the system. boomerAMG [39], is used with the following setup to solve the low order system:

- PMIS coarsening
- 0.25 strength threshold
- Extended + i interpolation ($p_{max} = 4$)
- L1 Jacobi smoothing
- One V-cycle for preconditioning
- Smoothing on the coarsest level

We denote this preconditioning strategy as SEMFEM.

5. High Order Cases. We describe four model problems that are used to test the high-order p -multigrid (pMG) preconditioners. The first is a stand-alone Poisson solve with the Kershaw mesh ($\varepsilon = 1, 0.3, 0.05$). The others are modest-scale NS problems, where the pressure Poisson problem is solved over 2,000 timesteps. Details regarding the spectral element discretization are given in [30]. The problem sizes are listed in Table 2 and range from small ($n=16M$ points) to moderate ($n=180M$).⁵

5.1. Poisson. The Kershaw family of meshes [18, 17] has been proposed as the basis for a high-order Poisson-solver benchmark by Center for Efficient Exascale Discretization (CEED) within the DOE Exascale Computing Project (ECP). This family is parameterized by an anisotropy measure, $\varepsilon = \varepsilon_y = \varepsilon_z \in (0, 1]$, that determines the degree of deformation in the y and z directions. As ε decreases, the mesh deformation and aspect ratio increase along with it. The Kershaw mesh is shown in Figure 5 for $\varepsilon = 1, 0.3, 0.05$. The domain $\Omega = [-1/2, 1/2]^3$ with Dirichlet boundary conditions on $\partial\Omega$. The right hand side for (1.1) is set to

$$(5.1) \quad f(x, y, z) = 3\pi^2 \sin(\pi x) \sin(\pi y) \sin(\pi z).$$

The linear solver terminates after reaching a relative residual reduction of 10^{-8} . For the 1st-Cheb, λ_{min}^{opt} smoother method, a random right-hand side is used to tune λ_{min} . The solver used is PGMRES(30) preconditioned with a single pMG V-cycle. Since this test case solves the Poisson equation, there is no timestep needed for the model problem.

⁵Larger cases for full-scale runs on Summit with $n=51B$ are reported in [14].

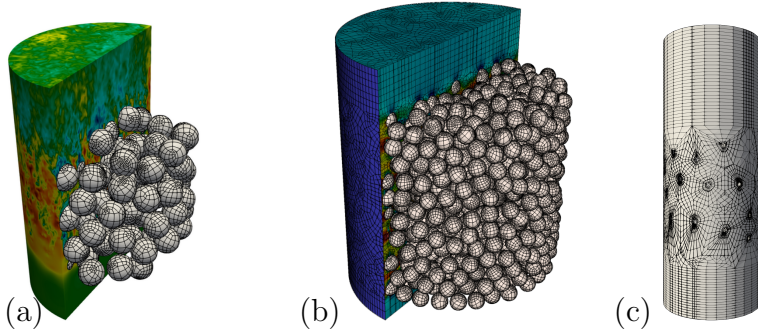


Fig. 6: Navier-Stokes cases: pebble-beds with (a) 146, (b) 1568, and (c) 67 spheres

Case	E	p	n	P	$\frac{n}{P}$
Kershaw (Figure 5)	47K	7	16M	6	2.6M
146 pebble (Figure 6a)	62K	7	21M	6	3.5M
1568 pebble (Figure 6b)	524K	7	180M	72	2.5M
67 pebble (Figure 6c)	122K	7	42M	18	2.3M

Table 2: Problem discretization parameters.

5.2. Navier-Stokes. For the pressure-Poisson tests, three flow cases are considered, as depicted in Figure 6. The first three cases corresponds to turbulent flow through a cylindrical packed-bed with 146, 1568, and 67 spherical pebbles. The 146 and 1568 pebble cases are from Lan and coworkers [20]. The 67 pebble case is constructed using an alternate Voronoi cell approach, and includes chamfers [31]. As such, the 67 pebble case is a more complex geometry. The first two bed flows are at Reynolds number $Re_D = 5000$, based on sphere diameter, D , while the 67 pebble case is at Reynolds number $Re_D = 1460$. Time advancement is based on a two-stage 2nd-order characteristics timestepper with CFL=4 ($\Delta t = 2 \times 10^{-3}$ $\Delta t = 5 \times 10^{-4}$, and $\Delta t = 5 \times 10^{-5}$ for the 146, 1568, and 67 pebble cases). An absolute pressure solver tolerance of 10^{-4} is used. A restart at $t = 10$, $t = 20$, and $t = 10$ convective time units is used for the 146, 1568, and 67 pebble cases, respectively, to provide an initially turbulent flow.

In all cases, solver results are collected over 2,000 timesteps. At each step, the solution is projected onto a space of up to 10 prior solution vectors to generate a high-quality initial guess, \bar{u} . Projection is standard practice in nekRS as it can reduce the initial residual by orders of magnitude at the cost of just two matrix-vector products in A per step [16]. The solver used is PGMRES(15) preconditioned with a single pMG V-cycle.

6. High Order Results. Here we consider the solver performance results for the test cases of section 5. We assign a single MPI rank to each GPU and denote the number of ranks as P . All runs are on Summit. Each node on Summit consists of 42 IBM Power9 CPUs and 6 NVIDIA V100 GPUs. Each case is preconditioned using pMG with a schedule of (7,5,3,1) for Jacobi-based and (7,3,1) for Schwarz-based Chebyshev smoothing. While $p = 1$ is treated as the coarse grid level for pMG, the problem sizes still scale linearly with the number of spectral elements.

6.1. Loss of Symmetry and PGMRES versus PCG. One concern regarding the one-sided V-cycle approach is the loss of symmetry in the preconditioner,

ε	PCG iter.	Time per PCG iter.	PGMRES iter.	Time per PGMRES iter.
1	20	1.26×10^{-2}	9	1.27×10^{-2}
0.3	286	1.38×10^{-2}	123	1.50×10^{-2}
0.05	1000	1.39×10^{-2}	474	1.52×10^{-2}

Table 3: Comparison of PCG and PGMRES(30) for the Kershaw cases using 1st-Cheb, Jacobi(3,3), (7,5,3,1) as preconditioner.

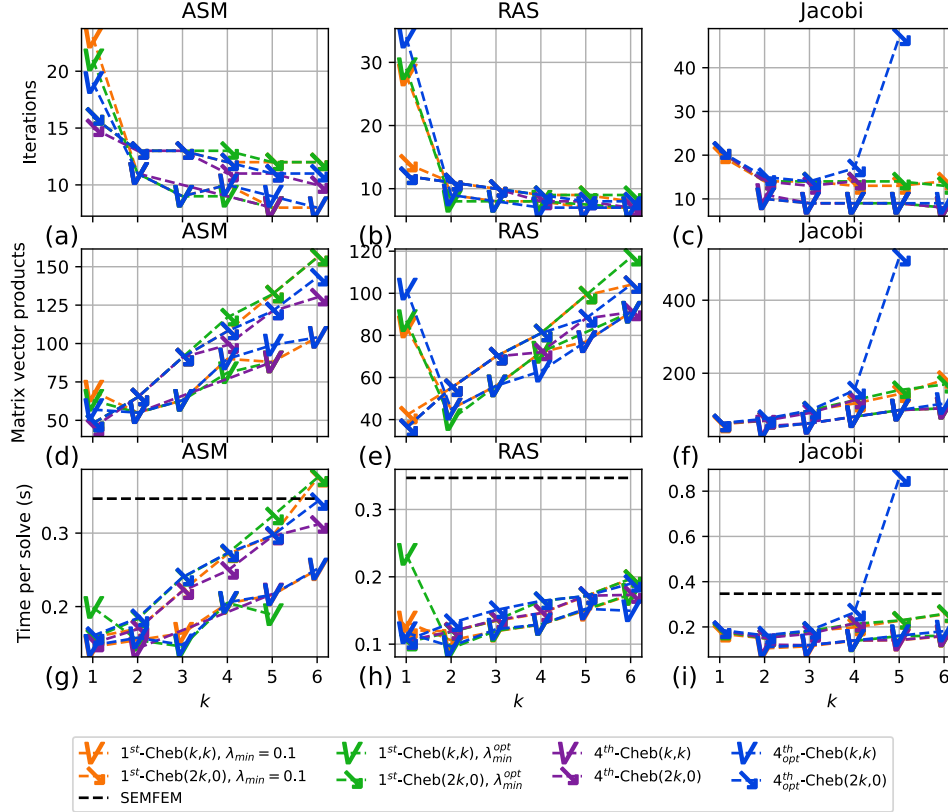
requiring the use of PGMRES instead of PCG as a KSP solver. There are, however, several strategies to mitigate this issue. Using restarted PGMRES(m) bounds the orthogonalization cost for n degrees of freedom to at most $O(m^2n)$ per iteration. Further, an effective preconditioning strategy can reduce this cost further by ensuring that k is small. An additional concern using PGMRES(m) is the $O(m)$ all-reduce operations per iteration. However, by utilizing classical Gram-Schmidt orthogonalization, PGMRES(m) requires only two all-reduce operations per iteration. Concerns over the loss of orthogonality are avoided by keeping m small (e.g., $m = 15$ or $m = 30$). While not used in this current work, Thomas and coworkers demonstrated that post-modern GMRES reduces the number of synchronizations to a single all-reduce while preserving backward stability [37].

Kershaw (subsection 5.1) results utilizing 1st Cheb, Jacobi(3,3), (7,5,3,1), pMG as a *symmetric* preconditioner with PCG and PGMRES(30) as the KSP solvers are shown in Table 3. Since the Kershaw case described in subsection 5.1 uses a 10^{-8} residual reduction for the convergence criterion of the solver, it follows that PGMRES should yield a lower iteration count than PCG. This is because PCG minimizes the A -norm of the error vector, while PGMRES minimizes the L_2 -norm of the error vector [33]. A more meaningful convergence criteria would be on the L_2 -norm of the error vector, however, this would not be known. As such, the results presented in Table 3 are meant to illustrate that the time to apply a single PGMRES iteration is similar to PCG. Consider that, for this case, PGMRES(30) is employed, thereby *over-estimating* the cost per iteration for the NS cases wherein PGMRES(15) is used. Lastly, the most effective preconditioning strategies utilize Schwarz-based Chebyshev smoothing. The ASM and RAS methods considered herein are *asymmetric*, and thus are not suitable for use with PCG.

6.2. Kershaw Results. Results for the Kershaw case for $\varepsilon = 1, 0.05$ are shown in Figure 7 and Figure 8, respectively ⁶. To mitigate the effects of system noise, the reported solve times are based on minimum time to solution over 50 trials. The reported number of matrix-vector products are for the *finest grid*, $p = 7$.

When $\varepsilon = 1$, the time to solution is minimized by utilizing a symmetric V-cycle with relatively low-order Chebyshev-accelerated RAS smoothing. For this case, SEMFEM is a comparatively poor method. While the iteration count is decreased with respect to increasing order, the overall cost of applying the heavier smoother translates to a higher cost per solve. This can especially be observed in the increased work requirement in terms of matrix-vector products, Figure 7d-f. At larger scales, however, the scalability of the AMG coarse grid solve may dominate the cost of the preconditioner, and thus anything to reduce the number of coarse grid solves may prove beneficial. In this scenario one should expect the multigrid approximation

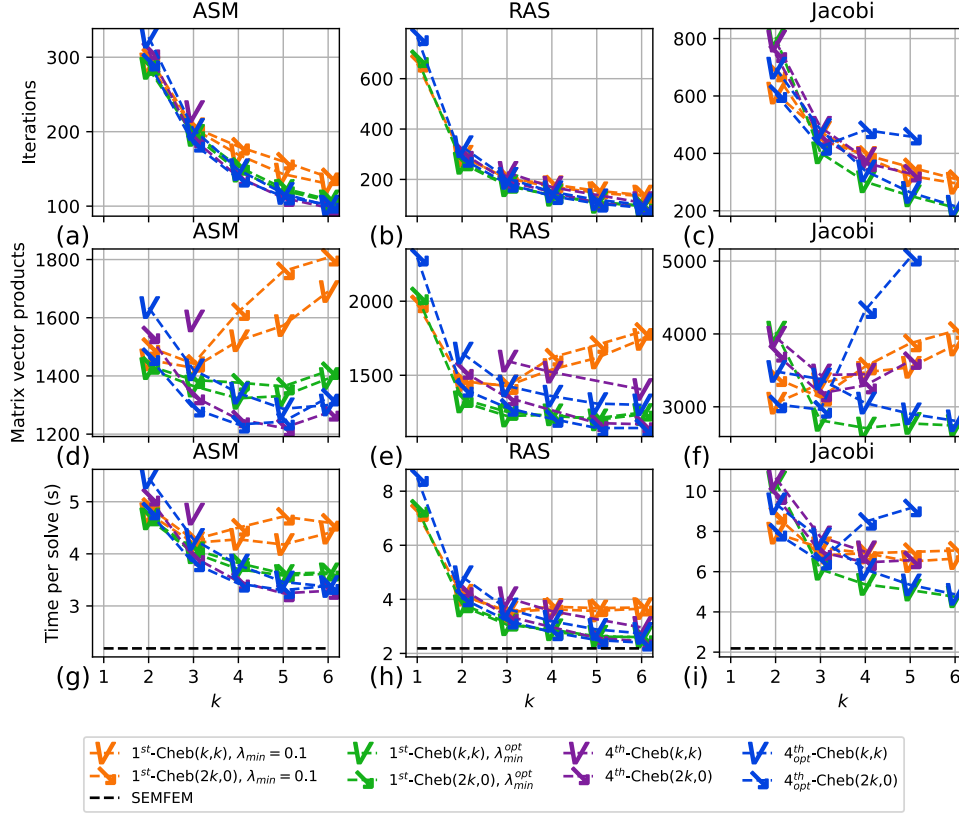
⁶ $\varepsilon = 0.3$ is in supplementary material as Figure 19. Additional plots showing a break down of the coarse grid solve timings are included in the supplementary material, Figure 20, Figure 21, and Figure 22.

Fig. 7: Kershaw results, $\varepsilon = 1$.

property constant(2.3) to be quite low for the case with no geometric deformation. In this regime, the theoretical prediction in Figure 1, states that the convergence is improved using a full V-cycle with k order Chebyshev smoothing as opposed to the half V-cycle with $\tilde{k} = 2k$ order presmoothing. Benchmarking demonstrates that a single boomerAMG V-cycle iteration for $p = 1$ on the CPU is nearly 12 times the cost of a matrix-vector product. For larger cases, wherein the number of AMG levels needed for a single boomerAMG V-cycle increases, the relative cost of the coarse grid solve will increase relative to the cost of a matrix-vector product.

For $\varepsilon = 0.05$, the fastest time to solution is reached using SEMFEM preconditioning. The pMG methods are significantly more expensive. For the 4th and opt. 4th-kind Chebyshev-accelerated RAS schemes considered, the time to solution is lowered by increasing the order. Remarkably, the 4th-kind and optimized 4th-kind Chebyshev schemes are generally equivalent to, if not better than, optimizing the λ_{min} parameter for the standard 1st Chebyshev scheme. This allows for increased performance with high order Chebyshev smoothing, without the requirement of tuning an additional parameter.⁷ Further, with the extreme geometric deformation, the multigrid approximation property constant(2.3) is expected to be quite large for this case. The results in Figure 1 predict that the one-sided approach yields a better convergence rate. The results confirm this theoretical expectation.

⁷In large-scale fluid mechanics applications, this overhead is easily amortized over the 10^4 – 10^6 timesteps required. Reasonably good values of λ_{min}^{opt} do not depend on the RHS, allowing this to be part of the setup cost of the preconditioner.

Fig. 8: Kershaw results, $\varepsilon = 0.05$.

A summary of the results for the Kershaw case is shown in Table 4. This table reports the solver yielding the lowest time to solution (in seconds), T_S , the iteration count, and the speedup over the time to solution of the default nekRS solver, T_D . The ratio between the time spent doing coarse grid solves for the default solver, $(T_{crs})_D$, and the time spent doing coarse grid solves for the fastest solver, $(T_{crs})_S$, is reported. The default nekRS solver is 1st-Cheb, ASM(3,3),(7,3,1). For the Kershaw case, these tables demonstrate that optimizing λ_{min} in the 1st-kind Chebyshev scheme greatly improves the solver performance⁸. While $\varepsilon = 1, 0.3$ do not benefit from the use of a one-sided V-cycle, the use of the one-sided V-cycle, in conjunction with the optimized 4th-kind Chebyshev smoother, is able to increase the solver speedup relative to the default solver by another 13% for $\varepsilon = 0.05$. A 75% speedup is achieved over the default solver for $\varepsilon = 1, 0.05$. For $\varepsilon = 0.3$, a much more modest 35% is achieved.

6.3. Navier-Stokes. Results for the 1568 and 67 pebble cases are shown in Figure 9 and Figure 10, respectively⁹. Since the 4th and optimized 4th-kind Chebyshev smoothers are comparable to the 1st-kind Chebyshev smoother with optimized λ_{min}

⁸A record of the optimal λ_{min}^{opt} values for the 1st-kind Chebyshev smoother are reported in the supplementary material, Figure 23. For hard problems (i.e., lower ε values), $\lambda_{min} = 1/20$. For easy problems, however, $\lambda_{min} = 3/20$ is reasonable.

⁹146 pebble results are shown in the supplementary material, Figure 24. Additional plots showing a break down of the coarse grid solve timings are included in the supplementary material, Figure 25, Figure 26, and Figure 27.

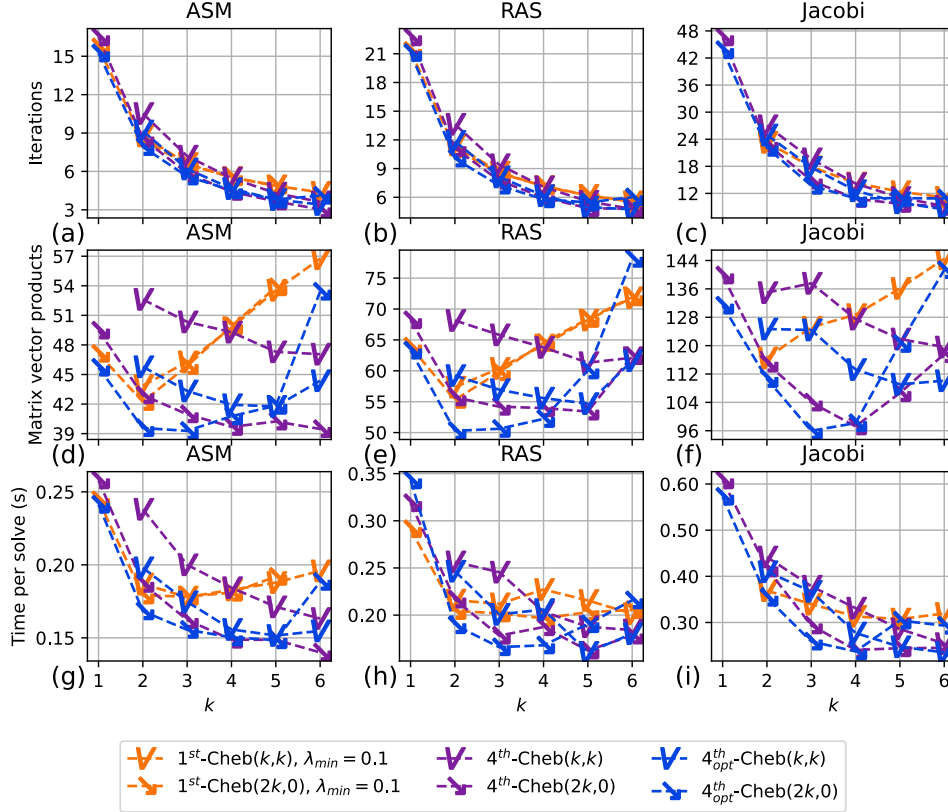


Fig. 9: 1568 pebble results.

as shown in subsection 6.2, this smoother is omitted from these cases.

The lowest time to solution for the 1568 pebble case is achieved using 4th-Cheb, ASM(12,0), Table 4. Figure 9d,g shows that the number of matrix-vector products remains nearly constant with respect to the order, yielding a lower time to solution by minimizing the coarse grid cost. The performance of the 1st-kind Chebyshev smoother, however, plateaus around $k = 3, k = 6$, especially for the Schwarz-based smoothers, see Figure 9g,h. Although some improvement is observed through the use of the half V-cycle, an additional benefit is observed by using the alternate Chebyshev smoothers from Lottes's work [22]. Without the added benefit of the one-sided V-cycle, the fastest solver for this case yields a 17% speedup over the default. However, enabling this half V-cycle approach further increases the solver performance to a 27% speedup over the default solver (Table 4).

The 67 pebble case is distinct from the other two pebble meshes. The 146 and 1568 pebble cases are meshed using an all-hex meshing strategy developed by Lan and coworkers [20]. The 67 pebble case includes chamfers, and is meshed using an alternate Voronoi cell approach [31]. The resulting mesh proves to be much more challenging for the pMG based strategies. Nevertheless, pMG with one-sided Chebyshev smoothing prove promising for this case. The time to solution is minimized at relatively high orders with RAS-based Chebyshev. This is further improved through the use of the half V-cycle. The *total work* required per solve is reduced at higher orders for the Schwarz-based approaches. Through tuning the pMG parameters, a significant speedup of 81% is achieved over the default solver. In this case, the fastest pMG

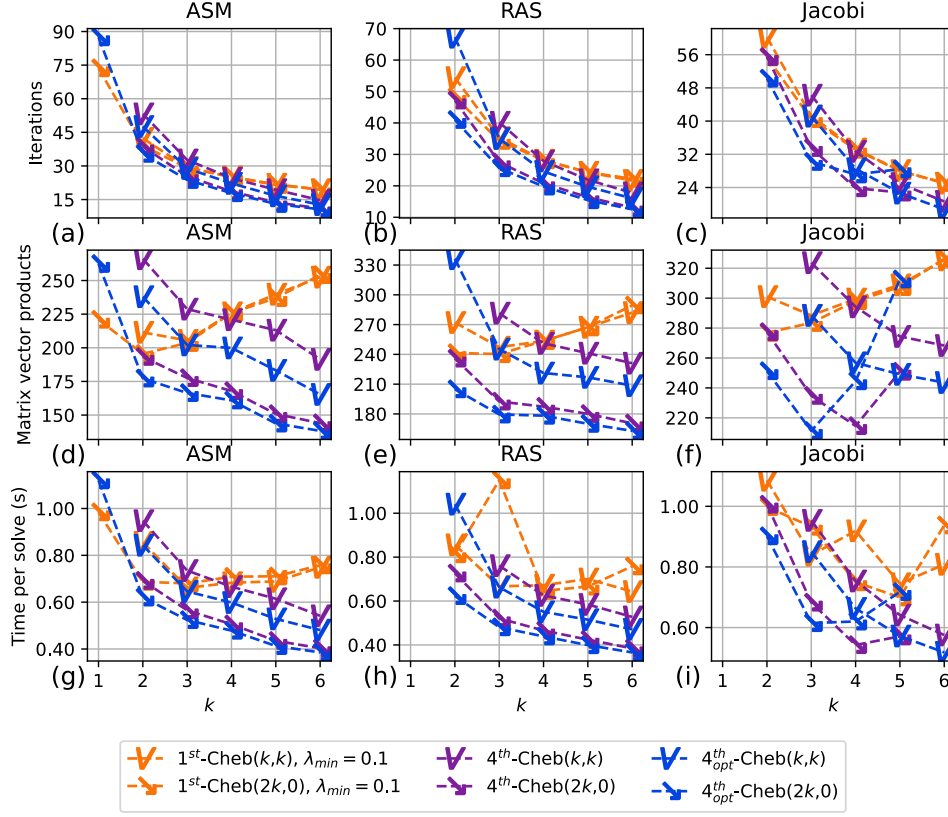


Fig. 10: 67 pebble results.

Case	Fastest Solver	T_S	Iterations	$\frac{T_D}{T_S}$	$\frac{(T_{crs})_D}{(T_{crs})_S}$
Kershaw ($\varepsilon = 1$)	1^{st} -Cheb, λ_{min}^{opt} , RAS(2,2)	0.09	8	1.75	1.13
Kershaw ($\varepsilon = 0.3$)	1^{st} -Cheb, λ_{min}^{opt} , RAS(5,5)	0.67	28	1.35	1.79
Kershaw ($\varepsilon = 0.05$)	4^{th}_{opt} -Cheb, RAS(12,0)	2.40	88	1.75	2.31
146 pebble	4^{th}_{opt} -Cheb, RAS(4,4)	0.15	5.3	1.17	1.21
67 pebble	4^{th}_{opt} -Cheb, RAS(12,0)	0.37	12.5	1.81	2.41
1568 pebble	4^{th} -Cheb, ASM(12,0)	0.14	3	1.27	2.13

Table 4: Solver configuration with the fastest time to solution.

preconditioner is 4^{th}_{opt} -Cheb, RAS(12,0).

7. Conclusions. In this work, we explore the use of one-sided V-cycle using Chebyshev smoothing as a preconditioner, both in a 2D finite difference example, as well as a PMG preconditioner for the pressure Poisson equation arising from the spectral element discretization of the NS equation. Further, we explore the efficacy of novel Chebyshev smoothers based on the work of Lottes [22] and demonstrate their improvement over the 1st-kind Chebyshev smoothers. This improvement enables increased solver performance, especially at high Chebyshev degrees. The benefit to this approach is further decreasing the coarse grid cost.

The authors plan on applying the Lottes's novel Chebyshev smoothers to AMG solvers. The application of this work are two fold. First, improved AMG solvers

will benefit the low-order SEMFEM preconditioning strategy for high-order finite elements. Secondly, improvements in AMG solvers will benefit the overall solver community. The authors also plan on applying the ideas developed herein to larger problems.

Acknowledgments. This research is supported by the Exascale Computing Project (17-SC-20-SC), a collaborative effort of two U.S. Department of Energy organizations (Office of Science and the National Nuclear Security Administration) responsible for the planning and preparation of a capable exascale ecosystem, including software, applications, hardware, advanced system engineering and early testbed platforms, in support of the nation’s exascale computing imperative. This research also used resources of the Oak Ridge Leadership Computing Facility at Oak Ridge National Laboratory, which is supported by the Office of Science of the U.S. Department of Energy under Contract DE-AC05-00OR22725.

The authors thank YuHsiang Lan, David Alan Reger, and Haomin Yuan for providing visualizations and mesh files.

REFERENCES

- [1] M. ADAMS, M. BREZINA, J. HU, AND R. TUMINARO, *Parallel multigrid smoothing: polynomial versus gauss–seidel*, Journal of Computational Physics, 188 (2003), pp. 593–610.
- [2] A. H. BAKER, R. D. FALGOUT, T. V. KOLEV, AND U. M. YANG, *Multigrid smoothers for ultraparallel computing*, SIAM Journal on Scientific Computing, 33 (2011), pp. 2864–2887.
- [3] P. D. BELLO-MALDONADO AND P. F. FISCHER, *Scalable low-order finite element preconditioners for high-order spectral element poisson solvers*, SIAM Journal on Scientific Computing, 41 (2019), pp. S2–S18.
- [4] A. BIENZ, W. D. GROPP, AND L. N. OLSON, *Reducing communication in algebraic multigrid with multi-step node aware communication*, The International Journal of High Performance Computing Applications, 34 (2020), pp. 547–561.
- [5] X.-C. CAI AND M. SARKIS, *A restricted additive schwarz preconditioner for general sparse linear systems*, Siam journal on scientific computing, 21 (1999), pp. 792–797.
- [6] N. CHALMERS, A. KARAKUS, A. P. AUSTIN, K. SWIRYDOWICZ, AND T. WARBURTON, *libParanumal: a performance portable high-order finite element library*.
- [7] T. CHAN AND W. WAN, *Analysis of projection methods for solving linear systems with multiple right-hand sides*, SIAM J. Sci. Comput., 18 (1997), pp. 1698–1721.
- [8] M. DEVILLE, P. FISCHER, AND E. MUND, *High-order methods for incompressible fluid flow*, Cambridge University Press, Cambridge, 2002.
- [9] R. D. FALGOUT AND J. B. SCHRODER, *Non-galerkin coarse grids for algebraic multigrid*, SIAM Journal on Scientific Computing, 36 (2014), pp. C309–C334.
- [10] N. FEHN, P. MUNCH, W. A. WALL, AND M. KRONBICHLER, *Hybrid multigrid methods for high-order discontinuous galerkin discretizations*, Journal of Computational Physics, 415 (2020), p. 109538.
- [11] N. FEHN, W. WALL, AND M. KRONBICHLER, *Efficiency of high-performance discontinuous Galerkin spectral element methods for under-resolved turbulent incompressible flows*, Int. J. Numer. Methods Fluids, (2018).
- [12] P. FISCHER, *An overlapping Schwarz method for spectral element solution of the incompressible Navier-Stokes equations*, J. Comput. Phys., 133 (1997), pp. 84–101.
- [13] P. FISCHER, S. KERKEMEIER, M. MIN, Y.-H. LAN, M. PHILLIPS, T. RATHNAYAKE, E. MERZARI, A. TOMBOULIDES, A. KARAKUS, N. CHALMERS, ET AL., *Nekrs, a gpu-accelerated spectral element navier-stokes solver*, preprint arXiv:2104.05829, (2021).
- [14] P. FISCHER, E. MERZARI, M. MIN, S. KERKEMEIER, Y.-H. LAN, M. PHILLIPS, T. RATHNAYAKE, A. NOVAK, D. GASTON, N. CHALMERS, ET AL., *Highly optimized full-core reactor simulations on summit*, preprint arXiv:2110.01716, (2021).
- [15] P. FISCHER, N. MILLER, AND H. TUFO, *An overlapping Schwarz method for spectral element simulation of three-dimensional incompressible flows*, in Parallel Solution of Partial Differential Equations, P. Bjørstad and M. Luskin, eds., Berlin, 2000, Springer, pp. 158–180.
- [16] P. F. FISCHER, *Projection techniques for iterative solution of $ax=b$ with successive right-hand sides*, Computer methods in applied mechanics and engineering, 163 (1998), pp. 193–204.
- [17] D. S. KERSHAW, *Differencing of the diffusion equation in lagrangian hydrodynamic codes*, Jour-

- nal of Computational Physics, 39 (1981), pp. 375–395.
- [18] T. KOLEV, P. FISCHER, A. AUSTIN, A. BARKER, N. BEAMS, J. BROWN, J. CAMIER, N. CHALMERS, V. DOBREV, Y. DUDOUIT, ET AL., *Ceed ecg milestone report: High-order algorithmic developments and optimizations for large-scale gpu-accelerated simulations*, tech. report.
 - [19] M. KRONBICHLER AND K. LJUNGKVIST, *Multigrid for matrix-free high-order finite element computations on graphics processors*, ACM Transactions on Parallel Computing, 6 (2019), pp. 1–32.
 - [20] Y.-H. LAN, P. FISCHER, E. MERZARI, AND M. MIN, *All-hex meshing strategies for densely packed spheres*, preprint arXiv:2106.00196, (2021).
 - [21] S. LOISEL, R. NABBEN, AND D. B. SZYLD, *On hybrid multigrid-schwarz algorithms*, Journal of Scientific Computing, 36 (2008), pp. 165–175.
 - [22] J. LOTTES, *Optimal polynomial smoothers for multigrid v-cycles*, preprint arXiv:2202.08830, (2022).
 - [23] J. W. LOTTES AND P. F. FISCHER, *Hybrid multigrid/schwarz algorithms for the spectral element method*, Journal of Scientific Computing, 24 (2005), pp. 45–78.
 - [24] R. LYNCH, J. RICE, AND D. THOMAS, *Direct solution of partial difference equations by tensor product methods*, Numer. Math., 6 (1964), pp. 185–199.
 - [25] S. McCORMICK, *Multigrid methods for variational problems: general theory for the v-cycle*, SIAM Journal on Numerical Analysis, 22 (1985), pp. 634–643.
 - [26] D. S. MEDINA, A. ST-CYR, AND T. WARBURTON, *Occa: A unified approach to multi-threading languages*, preprint arXiv:1403.0968, (2014).
 - [27] L. OLSON, *Algebraic multigrid preconditioning of high-order spectral elements for elliptic problems on a simplicial mesh*, SIAM Journal on Scientific Computing, 29 (2007), pp. 2189–2209.
 - [28] S. A. ORSZAG, *Spectral methods for problems in complex geometries*, in Numerical methods for partial differential equations, Elsevier, 1979, pp. 273–305.
 - [29] W. PAZNER, *Efficient low-order refined preconditioners for high-order matrix-free continuous and discontinuous galerkin methods*, SIAM Journal on Scientific Computing, 42 (2020), pp. A3055–A3083.
 - [30] M. PHILLIPS, S. KERKEMEIER, AND P. FISCHER, *Tuning spectral element preconditioners for parallel scalability on gpus*, in Proceedings of the 2022 SIAM Conference on Parallel Processing for Scientific Computing, SIAM, 2022, pp. 37–48.
 - [31] D. REGER, E. MERZARI, H. YUAN, S. KING, Y. HASSAN, K. NGO, P. BALESTRA, AND S. SCHUNERT, *Large eddy simulation of a 67-pebble bed experiment*, in Advances in Thermal-Hydraulics, June 2022.
 - [32] J. RUDI ET AL., *An extreme-scale implicit solver for complex pdes: highly heterogeneous flow in earth’s mantle*, in Proceedings of the international conference for high performance computing, networking, storage and analysis, 2015, pp. 1–12.
 - [33] Y. SAAD, *Iterative methods for sparse linear systems*, SIAM, 2003.
 - [34] J. STILLER, *Nonuniformly weighted schwarz smoothers for spectral element multigrid*, Journal of Scientific Computing, 72 (2017), pp. 81–96.
 - [35] K. STUBEN, *Algebraic multigrid (amg): an introduction with applications*, GMD report, (1999).
 - [36] H. SUNDAR, G. STADLER, AND G. BIROS, *Comparison of multigrid algorithms for high-order continuous finite element discretizations*, Numerical Linear Algebra with Applications, 22 (2015), pp. 664–680.
 - [37] S. THOMAS, E. CARSON, M. ROZLOŽNÍK, A. CARR, AND K. ŚWIRYDOWICZ, *Post-modern gmres*, preprint arXiv:2205.07805, (2022).
 - [38] O. WIDLUND, *Iterative substructuring methods: algorithms and theory for elliptic problems in the plane*, in First Int. Symposium on Domain Decomposition Methods for Partial Differential Equations, R. Glowinski, G. Golub, G. Meurant, and J. Périaux, eds., SIAM, 1988, pp. 113–128.
 - [39] U. M. YANG ET AL., *Boomeramg: A parallel algebraic multigrid solver and preconditioner*, Applied Numerical Mathematics, 41 (2002), pp. 155–177.

8. Supplementary Material.

8.1. Tabulated Coefficients for Optimized 4th-kind Chebyshev Smoother.

Values for β for the optimized 4th-kind Chebyshev smoother developed by Lottes are tabulate in Table 5.

8.2. Lanczos Algorithm for Estimating the Multigrid Approximation Property Constant. Modifying Lanczos iteration on $(SA)^{-1}$ to project onto the A -orthogonal complement of the coarse grid space, the multigrid approximation property constant is estimated by the Ritz value from the iteration shown in Algorithm 8.1.

Algorithm 8.1 Lanczos estimate of multigrid approximation property

```

 $\underline{q}_1 = \pi_f \text{ rand}, \underline{q}_1 = \underline{q}_1 / \|\underline{q}_1\|_2$ 
 $\underline{r} = \pi_f (SA)^{-1} \underline{q}_1$ 
 $\alpha_1 = \underline{q}_1^T \underline{r}$ 
 $\beta_1 = \|\underline{r}\|_2$ 
for  $k = 2, \dots, m$  do
     $\underline{q}_k = \underline{r} / \beta_{k-1}$ 
     $\underline{r} = \pi_f \left( (SA)^{-1} \underline{q}_k - \beta_{k-1} \underline{q}_{k-1} \right)$ 
     $\alpha_k = \underline{q}_k^T \underline{r}$ 
     $\beta_k = \|\underline{r}\|_2$ 
end for

return  $\rho \left( \begin{bmatrix} \alpha_1 & \beta_1 & & & \\ \beta_1 & \alpha_2 & \beta_2 & & \\ & \beta_2 & \alpha_3 & \ddots & \\ & & \ddots & \ddots & \beta_{m-1} \\ & & & \beta_{m-1} & \alpha_m \end{bmatrix} \right)$ 
```

8.3. Geometric Multigrid for Finite Differences. Geometric multigrid results comparing the ratio of the error contraction rate for the full V-cycle approach to the one-sided V-cycle approach are shown in Figure 11, Figure 12, Figure 13, and Figure 14 for the 1st, 1st with tuned λ_{min}^{opt} , 4th-kind Chebyshev smoother, and optimal 4th-kind Chebyshev smoother, respectively.

1st-Cheb, $\lambda_{min} = 0.1$

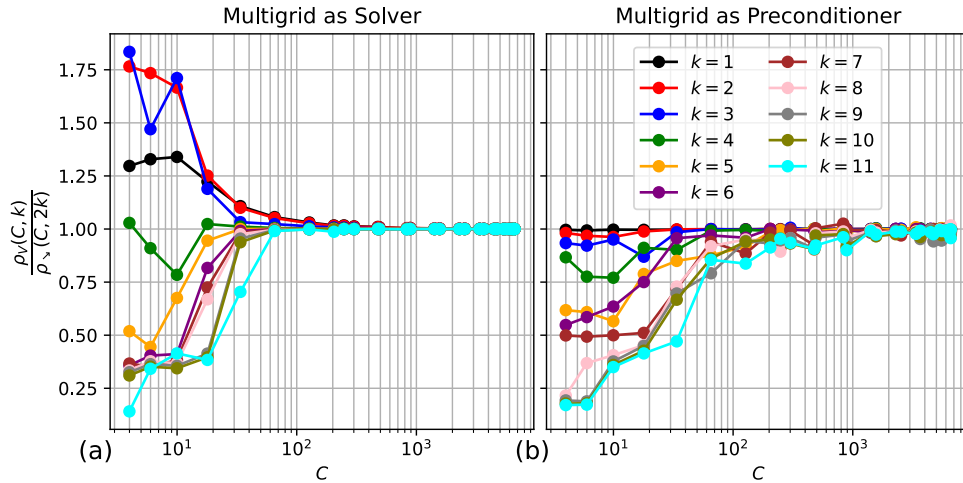


Fig. 11: Comparison of error contraction rates for the full V-cycle and the one-sided V-cycle for the 1st-kind Chebyshev smoother with $\lambda_{min} = 0.1$, based on finite difference results. Values larger than unity imply that the one-sided V-cycle is a better solver/preconditioner than the full V-cycle at the *same* cost per iteration.

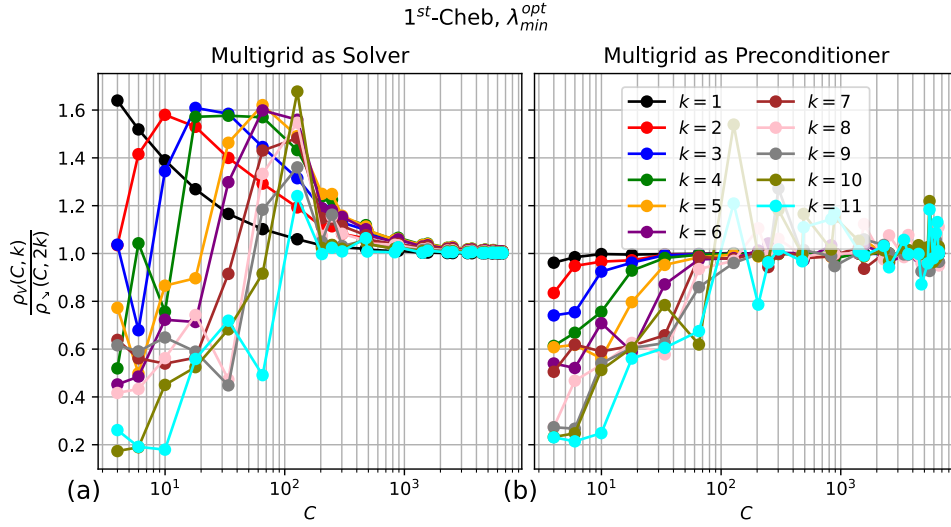


Fig. 12: Comparison of error contraction rates for the full V-cycle and the one-sided V-cycle for the 1st-kind Chebyshev smoother with optimized λ_{min} , based on finite difference results. Values larger than unity imply that the one-sided V-cycle is a better solver/preconditioner than the full V-cycle at the *same* cost per iteration.

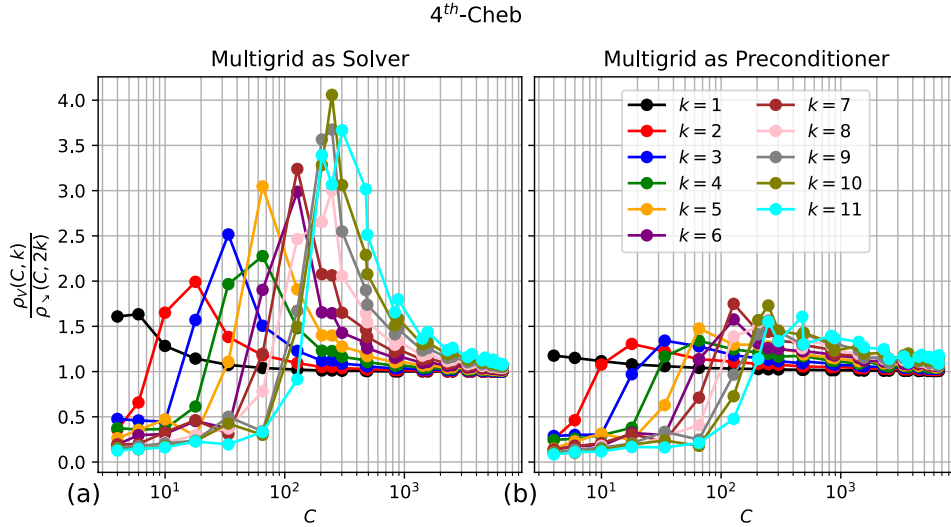


Fig. 13: Comparison of error contraction rates for the full V-cycle and the one-sided V-cycle for the 4th-kind Chebyshev smoother, based on finite difference results. Values larger than unity imply that the one-sided V-cycle is a better solver/preconditioner than the full V-cycle at the *same* cost per iteration.

Figure 15 shows the predicted and observed C^* the ratio between the one-sided and full V-cycle approaches is maximized or minimized. While the predicted C^* maximizer/minimizer of the ratio based on Lemma 2.1 is predictive when considering the usage of multigrid as a solver (Figure 15a), this is not necessarily the case for multigrid as a preconditioner. Remarkably, however, the C^* values predicted for 4th-

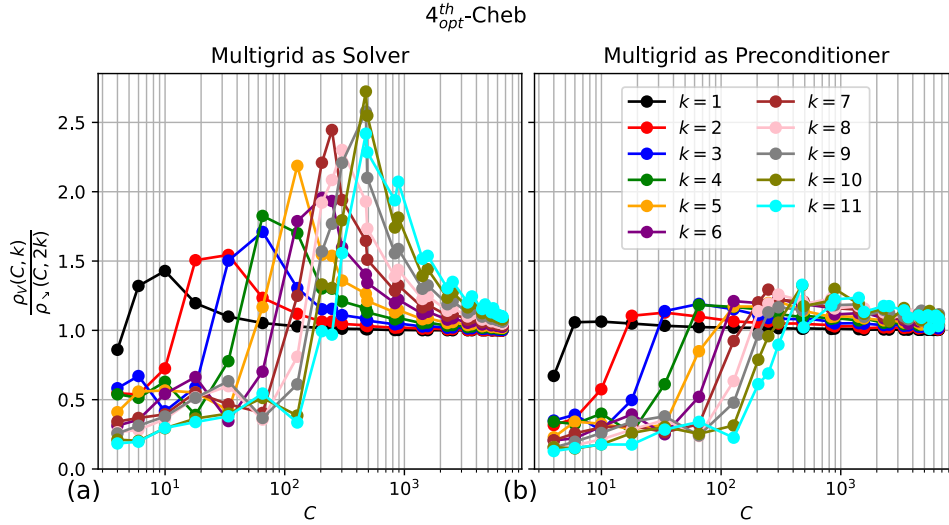


Fig. 14: Comparison of error contraction rates for the full V-cycle and the one-sided V-cycle for the optimized 4th-kind Chebyshev smoother, based on finite difference results. Values larger than unity imply that the one-sided V-cycle is a better solver/preconditioner than the full V-cycle at the *same* cost per iteration.

kind Chebyshev smoothers nevertheless match the experimental observation, even in the case of multigrid as a preconditioner.

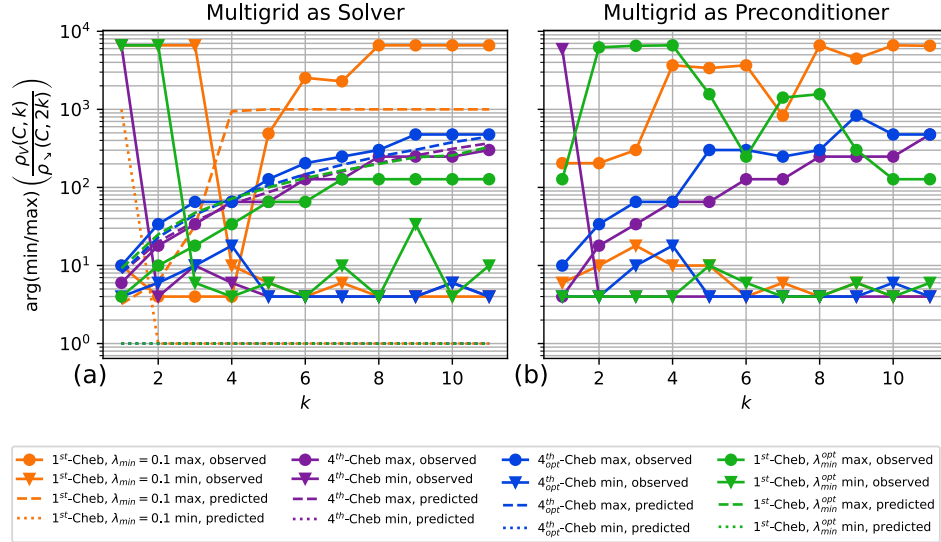
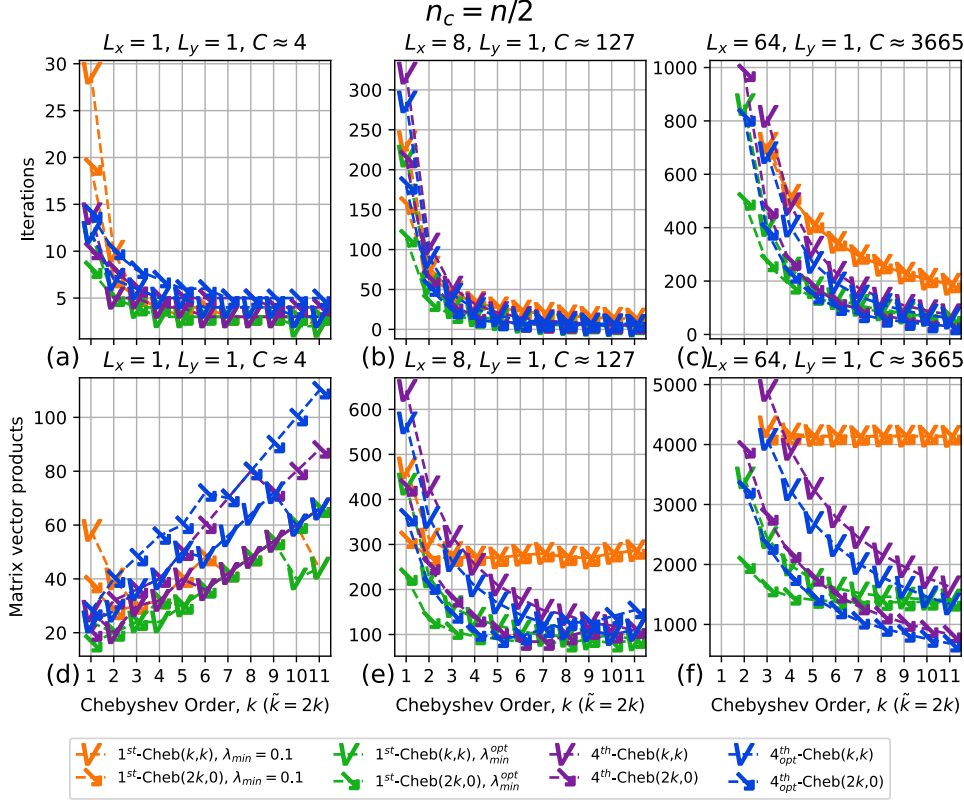


Fig. 15: C value that maximizes (minimizes) the error contraction rate ratios for the full V-cycle and the one-sided V-cycle, based on finite difference results. Predicted results are based on the error bounds provided by Lemma 2.1 (only applicable to multigrid as a solver, not preconditioner). Observed results are from 2D finite difference example.

Finite difference results, solved with geometric multigrid as a solver, rather than a preconditioner, are shown in Figure 16 and Figure 17 for the $n_c = n/2$ and $n_c = n/16$ cases, respectively.

Tuned values for λ_{min} for the 1st-kind Chebyshev smoother in Figure 18.

Fig. 16: FD, $n_c = n/2$. Multigrid is used as a *solver*.

8.4. Geometric p Multigrid for Pressure Poisson. Mesh quality metrics for the high-order cases are shown in Table 6.

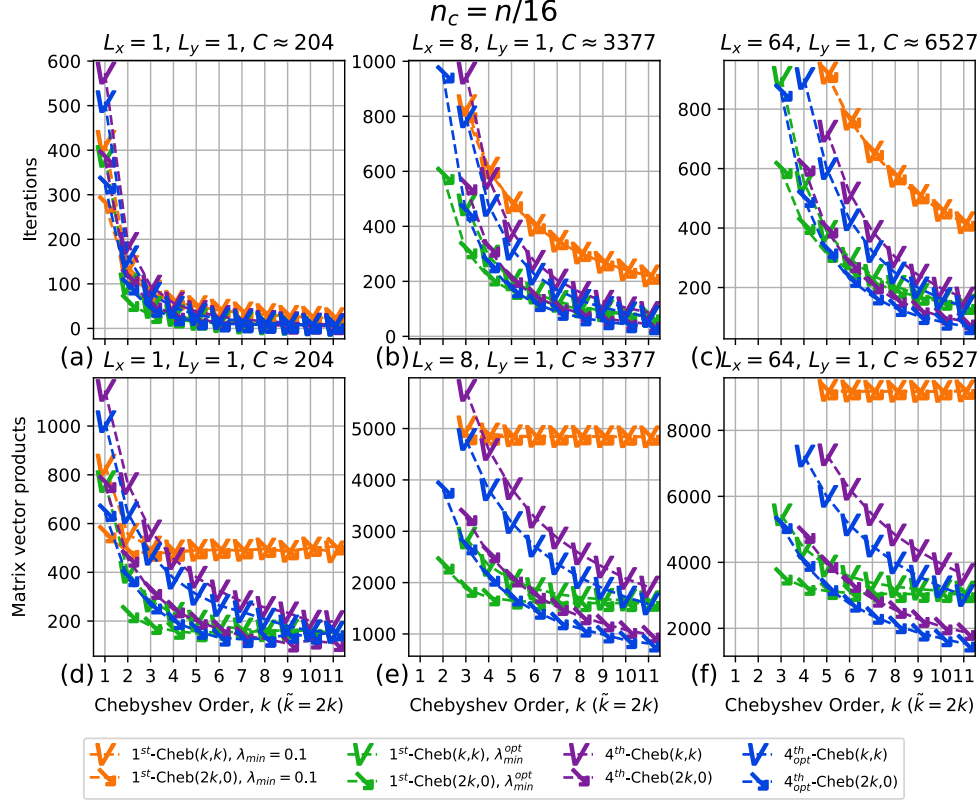
8.4.1. Poisson. Kershaw results for $\varepsilon = 0.3$ are shown in Figure 19. When $\varepsilon = 0.3$, however, higher-order Chebyshev smoothing can yield a lower time to solution. As shown in Figure 19d, the time to solution for the 4th and 4th_{opt} Chebyshev schemes tend to improve with high orders, even up to $k = 6$ for the full V-cycle (or $\tilde{k} = 12$ for the half V-cycle). This demonstrates a major improvement over the standard 1st Chebyshev scheme, which tends to yield a minimum time to solution at $k = 3$. Similar to the $\varepsilon = 1$ case, SEMFEM is not the preconditioner yielding the fastest time to solution. However, this approach becomes comparable to Jacobi-based Chebyshev smoothing.

pMG results for Kershaw (subsection 5.1) with $\varepsilon = 1, 0.3, 0.05$ are shown in Figure 20, Figure 21, and Figure 22, respectively. Here, the focus is on the tradeoff between using a heavier smoother versus additional coarse grid solves with a lighter smoother. The time per solve is additionally reported.

Values for $\lambda_{\min}^{\text{opt}}$ are shown in Figure 23. While the value depends on the specific case and order used, $\lambda_{\min} = 1/20$ is a reasonable value for problems with some amount of geometric deformation in the mesh.

8.4.2. Navier-Stokes. pMG results for the 146 pebble Navier-Stokes case mentioned in subsection 5.2 are shown in Figure 24.

pMG results for the Navier-Stokes cases mentioned in subsection 5.2 are shown

Fig. 17: FD, $n_c = n/16$. Multigrid is used as a *solver*.

in Figure 25, Figure 26, and Figure 27 for the 146, 1568, and 67 cases, respectively. Here, the focus is on the tradeoff between using a heavier smoother versus additional coarse grid solves with a lighter smoother. The time per solve is additionally reported.

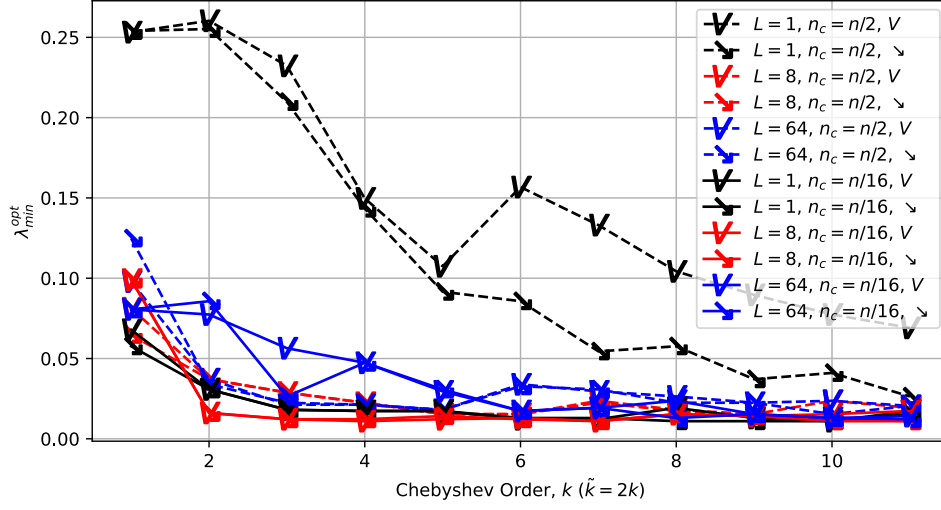


Fig. 18: Optimal 1st-kind λ_{min}^{opt} value from finite differences.

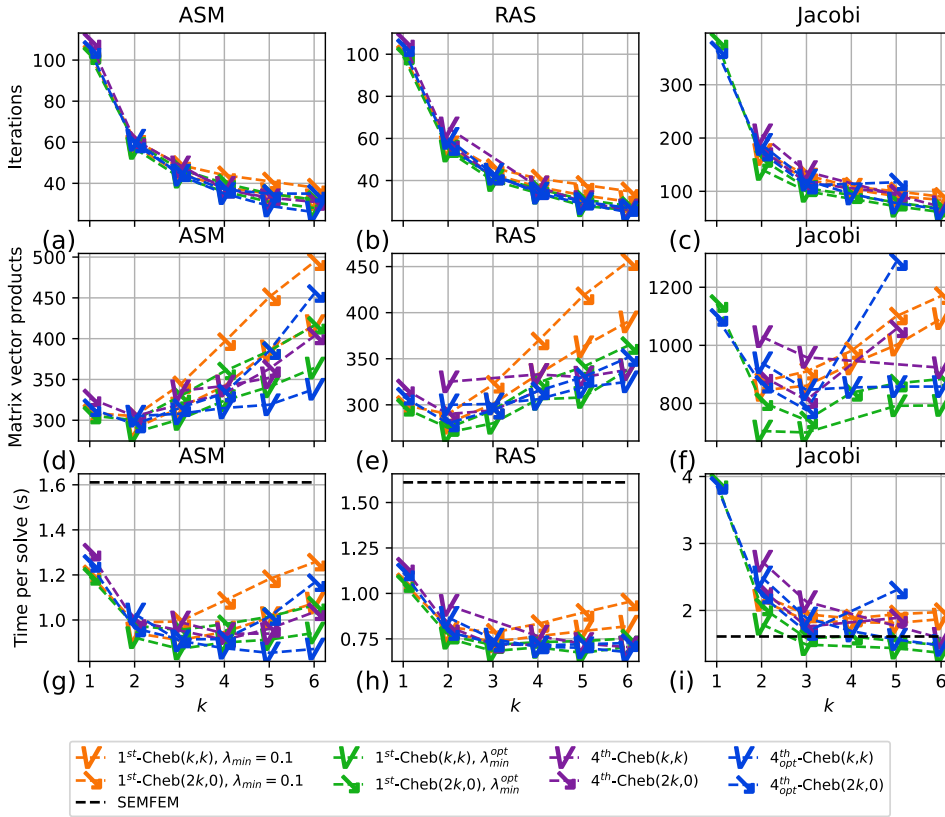


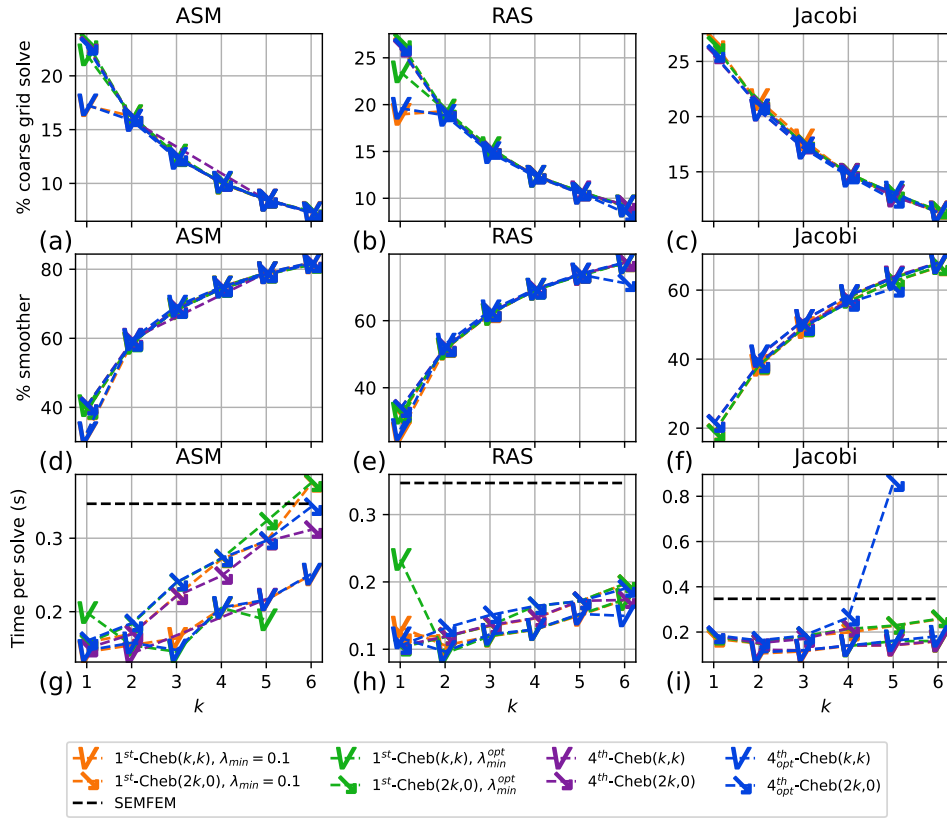
Fig. 19: Kershaw results, $\varepsilon = 0.3$.

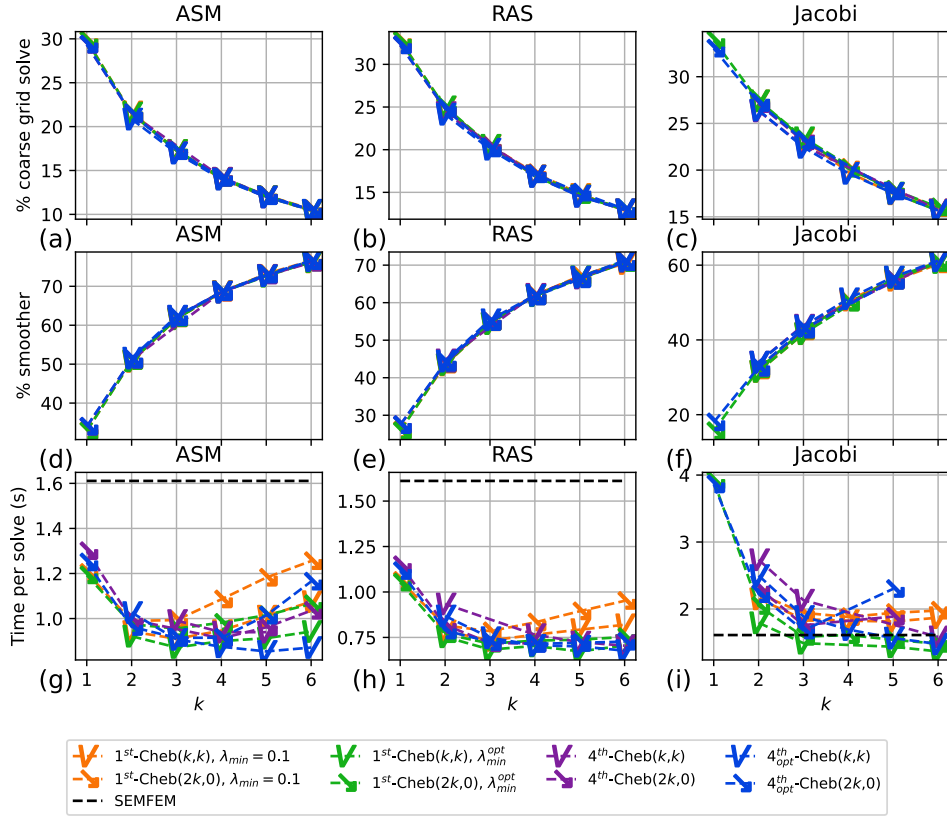
k	$\beta_i^{(k)}$	k	$\beta_i^{(k)}$	k	$\beta_i^{(k)}$
1	1.12500000000000	10	1.00030312229652	14	1.00011490538261
2	1.02387287570313		1.00304840660796		1.00115246376914
	1.26408905371085		1.01077022715387		1.00405357333264
3	1.00842544782028		1.02619011597640		1.00979590573153
	1.08867839208730		1.05231724933755		1.01941300472994
	1.33753125909618		1.09255743207549		1.03401425035436
4	1.00391310427285		1.15083376663972		1.05480599606629
	1.04035811188593		1.23172250870894		1.08311420301813
	1.14863498546254		1.34060802024460		1.12040891660892
	1.38268869241000		1.48386124407011		1.16833095655446
5	1.00212930146164	11	1.00023058595209		1.22872122288238
	1.02173711549260		1.00231675024028		1.30365305707817
	1.07872433192603		1.00817245396304		1.39546814053678
	1.19810065292663		1.01982986566342		1.50681646209583
	1.41322542791682		1.03950210235324	15	1.00009404750752
6	1.00128517255940		1.06965042700541		1.00094291696343
	1.01304293035233		1.11305754295742		1.00331449056444
	1.04678215124113		1.17290876275564		1.00800294833816
	1.11616489419675		1.25288300576792		1.01584236259140
	1.23829020218444		1.35725579919519		1.02772083317705
	1.43524297106744		1.49101672564139		1.04459535422831
7	1.00083464397912	12	1.00017947200828		1.06750761206125
	1.00843949430122		1.00180189139619		1.09760092545889
	1.03008707768713		1.00634861907307		1.13613855366157
	1.07408384092003		1.01537864566306		1.18452361426236
	1.15036186707366		1.03056942830760		1.24432087304475
	1.27116474046139		1.05376019693943		1.31728069083392
	1.45186658649364		1.08699862592072		1.40536543893560
8	1.00057246631197		1.13259183097913		1.51077872501845
	1.00577427662415		1.19316273358172	16	1.00007794828179
	1.02050187922941		1.27171293675110		1.00078126847253
	1.05019803444565		1.37169337969799		1.00274487974401
	1.10115572984941		1.49708418575562		1.00662291017015
	1.18086042806856	13	1.00014241921559		1.01309858836971
	1.29838585382576		1.00142906932629		1.02289448329337
	1.46486073151099		1.00503028986298		1.03678321409983
9	1.00040960072832		1.01216910518495		1.05559875719896
	1.00412439506106		1.02414874342792		1.08024848405560
	1.01460212148266		1.04238158880820		1.11172607131497
	1.03561113626671		1.06842008128700		1.15112543431072
	1.07139972529194		1.10399010936759		1.19965584614973
	1.12688273710962		1.15102748242645		1.25865841744946
	1.20785219140729		1.21171811910125		1.32962412656664
	1.32121930716746		1.28854264865128		1.41421360695576
	1.47529642820699		1.38432619380991		1.51427891730346
			1.50229418757368		

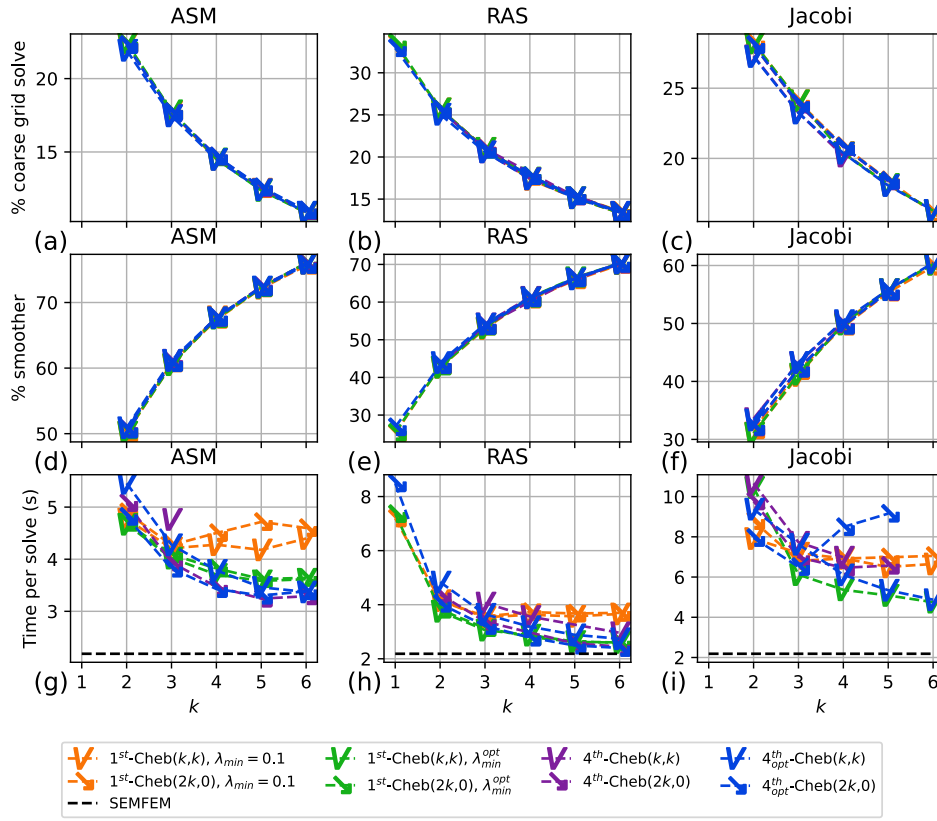
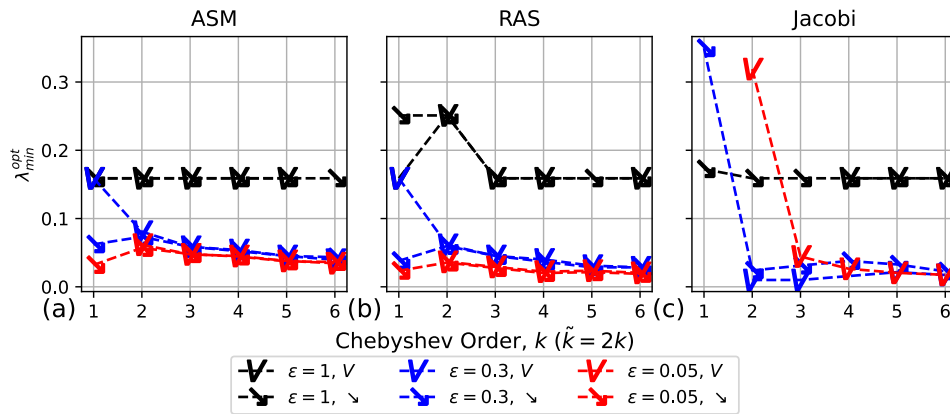
Table 5: Tabulated values of β for the optimized 4th-kind Chebyshev smoother.

Case Name	Scaled Jacobian (min/max/avg)	Aspect Ratio (min/max/avg)
Kerhsaw ($\varepsilon = 1$)	1 / 1 / 1	1 / 1 / 1
Kerhsaw ($\varepsilon = 0.3$)	0.316 / 1 / 0.841	1.08 / 20.1 / 4.64
Kerhsaw ($\varepsilon = 0.05$)	1.86×10^{-2} / 1 / 0.733	1.1 / 162 / 21.7
146 pebble	4.31×10^{-2} / .977 / .419	1.07 / 56.9 / 7.14
1568 pebble	2.59×10^{-2} / .99 / .371	1.12 / 108 / 12.6
67 pebble	5.97×10^{-3} / .970 / .38	1.17 / 204 / 13.2

Table 6: Mesh quality metrics for cases from Figure 5 and Figure 6.

Fig. 20: Kershaw results, $\varepsilon = 1$.

Fig. 21: Kershaw results, $\varepsilon = 0.3$.

Fig. 22: Kershaw results, $\varepsilon = 0.05$.Fig. 23: Optimal 1st-kind $\lambda_{\min}^{\text{opt}}$ value from Kershaw case.

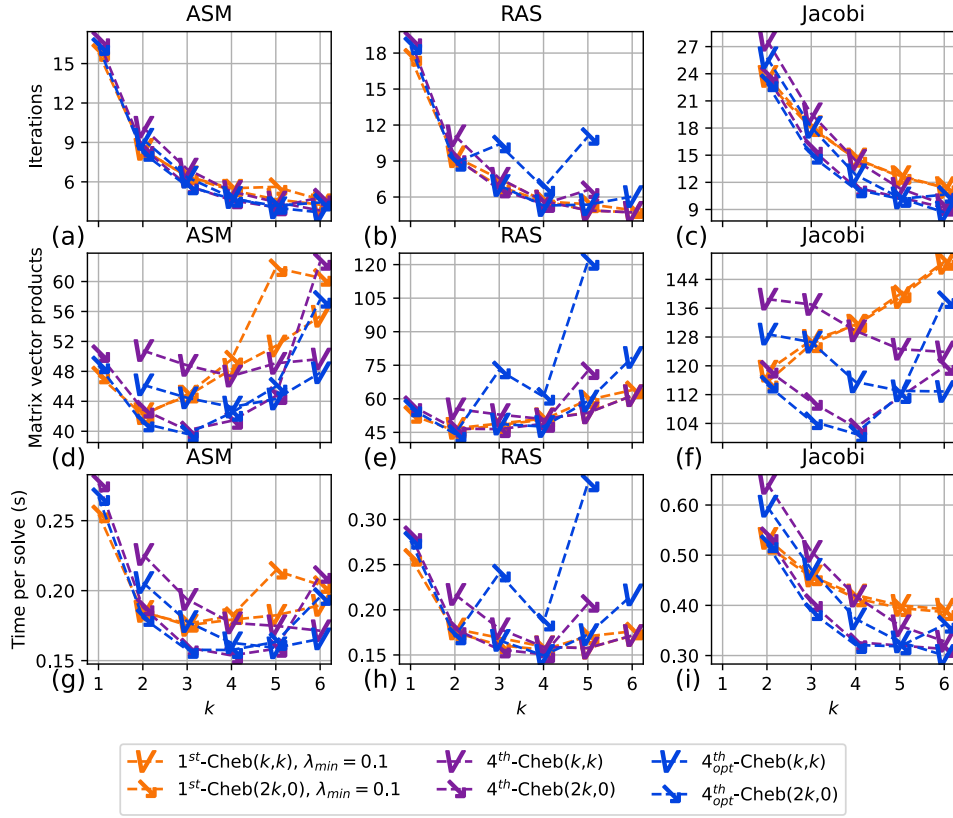


Fig. 24: 146 pebble results.

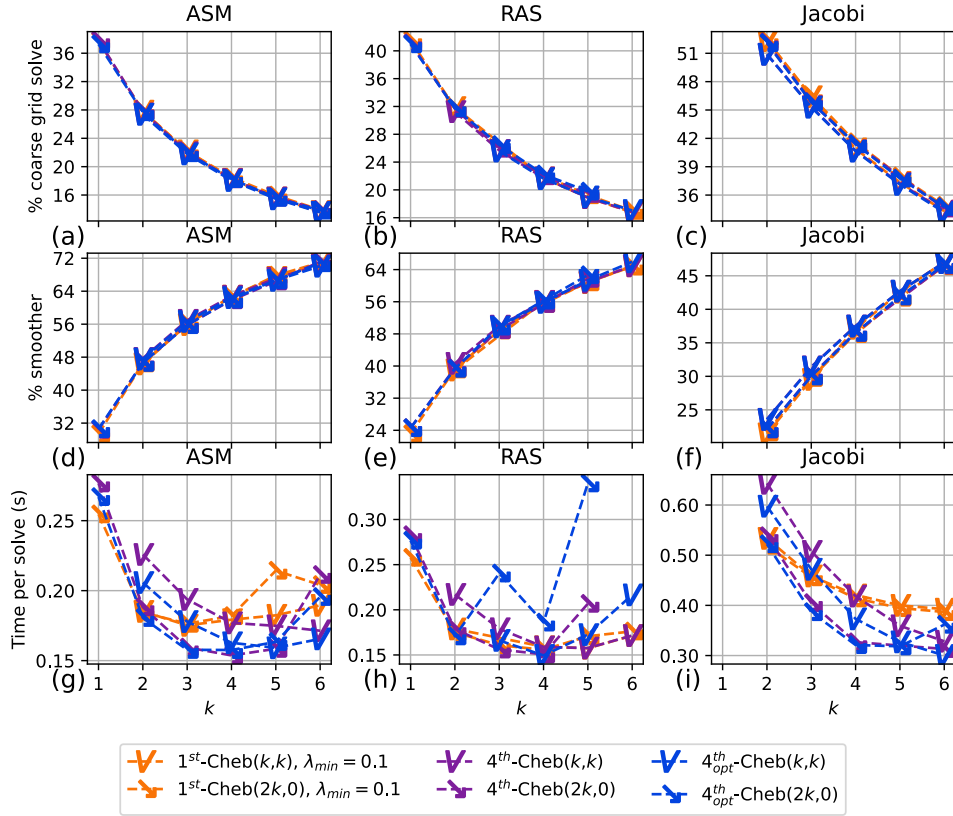


Fig. 25: 146 pebble results, including fraction spent in coarse grid solve versus smoother.

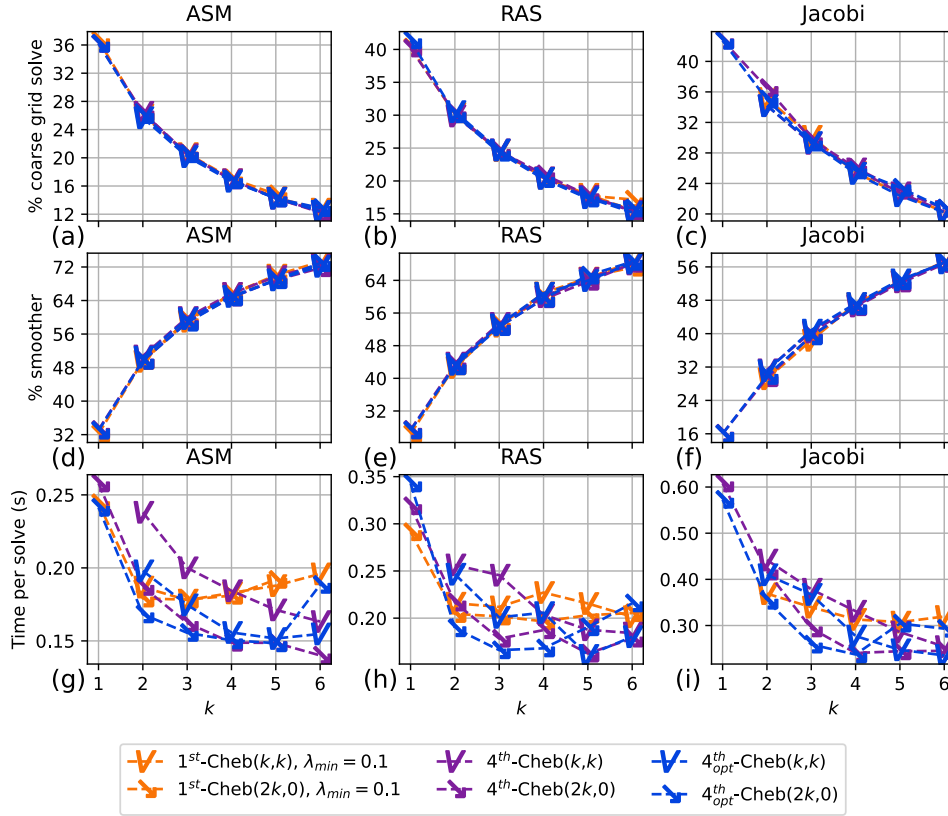


Fig. 26: 1568 pebble results, including fraction spent in coarse grid solve versus smoother.

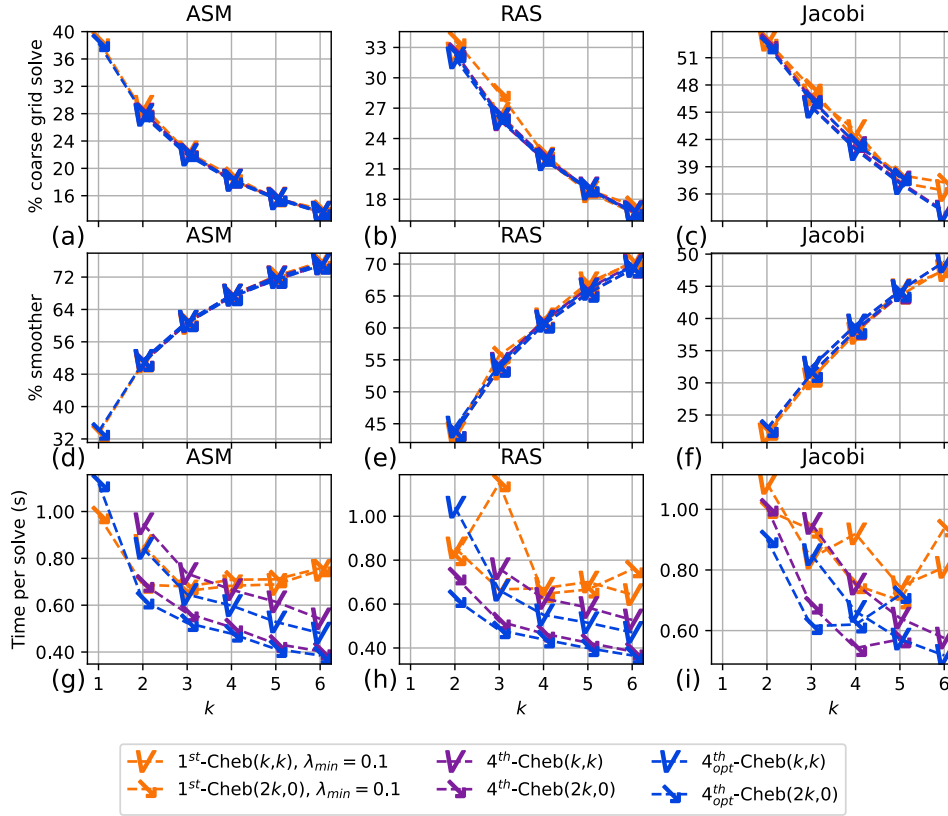


Fig. 27: 67 pebble results, including fraction spent in coarse grid solve versus smoother.